DIFFERENT ORBIT DETERMINATION ALGORITHMS FOR BILSAT-1

SERKAN URAL

JANUARY 2006

DIFFERENT ORBIT DETERMINATION ALGORITHMS FOR BILSAT-1

A THESIS SUBMITTED TO
THE GRADUATE SCHOOL OF NATURAL AND APPLIED SCIENCES
OF
MIDDLE EAST TECHNICAL UNIVERSITY

BY

SERKAN URAL

IN PARTIAL FULFILLMENT OF THE REQUIREMENTS
FOR
THE DEGREE OF MASTER OF SCIENCE
IN
GEODETIC AND GEOGRAPHICAL INFORMATION TECHNOLOGIES

JANUARY 2006

Approval of the Graduate School of Natural and Applied Sciences

Prof. Dr. Canan ÖZGEN
Director

I certify that this thesis satisfies all the requirements as a thesis for the degree of Master of Science.

Assist. Prof. Dr. Zuhal AKYÜREK
Head of Department

This is to certify that we have read this thesis and that in our opinion it is fully adequate, in scope and quality, as a thesis for the degree of Master of Science.

Assist. Prof. Dr. Mahmut Onur KARSLIOĞLU
Supervisor

Examining Committee Members

Assoc. Prof. Dr. Mustafa TÜRKER (Hacettepe U.,JFM) _____

Assist. Prof. Dr. M.Onur KARSLIOĞLU (METU,CE) _____

Assist. Prof. Dr. Utku KANOĞLU (METU,ES) _____

Dr. Jürgen FRIEDRICH (TÜBİTAK) _____

Gökhan YÜKSEL (TÜBİTAK) _____

I hereby declare that all information in this document has been obtained and presented in accordance with academic rules and ethical conduct. I also declare that, as required by these rules and conduct, I have fully cited and referenced all material and results that are not original to this work.

Name, Last name : Serkan URAL

Signature :

ABSTRACT

DIFFERENT ORBIT DETERMINATION ALGORITHMS FOR BILSAT-1

Ural, Serkan

MSc., Department of Geodetic And Geographic Information Technologies
Supervisor: Assist. Prof. M. Onur KARSLIOĞLU

January 2006, 76 pages

This study aims to investigate different orbit determination algorithms for the first Turkish remote sensing satellite, BİLSAT-1. The micro-satellite carries an onboard GPS receiver. Pseudorange measurements simulated from the position and velocity data supplied by TÜBİTAK-BİLTEN are used for the implementation of different orbit determination algorithms concluding to an estimate of the satellite's state.

Satellite's position, velocity components and the GPS receiver's clock bias are selected as the state parameters to be estimated. Kalman filter algorithms are used for the estimation of these state parameters. The modeled affecting force components include; geopotential and atmospheric drag. The global gravity models EGM96 and EIGEN-CG03C have been utilized together with Harris Priester atmospheric density model for the force modeling. The effect of the changes during the implementation of the force models, numerical integration, and estimation algorithms are investigated.

Software has been developed using MATLAB programming language for the implementation of all algorithms performed in this study for orbit determination.

Key Words: BİLSAT-1, orbit determination, kalman filter, GPS

ÖZ

BİLSAT-1 İÇİN FARKLI YÖRÜNGE BELİRLEME ALGORİTMALARI

Ural, Serkan

Yüksek Lisans, Jeodezi ve Coğrafi Bilgi Teknolojileri Bölümü
Tez Yöneticisi: Yrd.Doç.Dr. M. Onur KARSLIOĞLU

Ocak 2006, 76 sayfa

Bu çalışma ilk Türk uzaktan algılama uydusu BİLSAT-1 için farklı yörünge belirleme algoritmalarını araştırmayı amaçlamaktadır. Mikro-uydu, üzerinde bir adet GPS alıcısı taşımaktadır. TÜBİTAK-BİLTEN tarafından sağlanan konum ve hız verileri ile simulasyonu yapılan mesafe ölçümleri, uydunun durumunun kestirimiyle sonuçlanan farklı yörünge belirleme algoritmalarının uygulaması için kullanılmıştır.

Uydunun konum ve hız bileşenleri ile GPS alıcısının saat hatası kestirilecek durum parametreleri olarak seçilmiştir. Bu durum parametrelerinin kestirimi için Kalman filtre algoritmaları kullanılmıştır. Jeopotansiyel ve atmosferik sürükleme etkiyen kuvvet bileşenleri olarak modellenmiştir. Kuvvetlerin modellenmesinde EGM96 ve EIGEN-CG03C küresel yerçekimi modeli ile Harris Priester atmosfer yoğunluk modeli kullanılmıştır. Kuvvet modelleri, sayısal integrasyon, ve parametre kestirimi algoritmalarının uygulanması sırasında yapılan değişikliklerin etkileri incelenmiştir.

Bu çalışmada yörünge belirlemesi için kullanılan tüm algoritmaların uygulanması için MATLAB proglamlama dili kullanılarak bir yazılım geliştirilmiştir.

Anahtar Kelimeler: BİLSAT-1, yörünge belirleme, kalman filtresi, GPS

ACKNOWLEDGEMENTS

I would like to express my great appreciation to my supervisor, Asst. Prof. Dr. Mahmut Onur KARSLIOĞLU for the opportunities he provided and all the guidance and support throughout my research.

I would also like to thank to my friends Metin NOHUTCU and Halis BETTEMİR for all their contribution to the ideas and their suggestions which have been so valuable for the completion of this study.

I would like to thank to TÜBİTAK/BİLTEN for the data they provided which gave me the opportunity to perform all the investigations subject to my study.

I would like to thank to Assoc. Prof. Dr. Mustafa TÜRKER, Dr. Jürgen FRIEDRICH, Gökhan YÜKSEL and Assist. Prof. Dr. Utku KANOĞLU for believing in my determination on the subject and for all their patience.

I would like to express my gratitude to all my colleagues in BOTAŞ for all their support.

Finally, I would like to thank to my family for being with me whenever I needed.

TABLE OF CONTENTS

LIST OF TABLES

TABLE

LIST OF FIGURES

FIGURE

CHAPTER 1

INTRODUCTION

Artificial satellites, covering all around our planet each on their own paths have become integrated with a wide area of applications enlarging with a new contribution every day. The need for knowing the satellite's state consisting of its position and velocity at a specific instant of time with variable accuracy requirements depending on the purpose of the satellite is valid for all artificial satellites. A variety of techniques has emerged since the first satellite launched to its orbit and more techniques will surely be involved as far as the pursuit of higher efficiency exists.

In the early development of GPS, it was observed that the precise, global coverage and ease of use of GPS could significantly improve the determination of orbits of Low Earth Orbiters (Bisnath, 2004). Inclusion of the Global Positioning System (GPS) to orbit determination solution techniques enabling the tracking of the satellite's position by measurements from the GPS satellites brought an interesting area of investigation. When compared to the ground based tracking alternatives, larger observation capabilities of the system help it to become a more attractive area of research for better performance.

There are various orbit determination strategies in which the GPS observables are involved. In this study, it is aimed to investigate different algorithms with simulated pseudorange observables of the GPS receiver on board the first Turkish remote sensing micro-satellite BİLSAT-1. The position and velocity data of Bilsat-1 obtained from TÜBİTAK-BİLTEN has been used to simulate pseudorange observables in order to be used for orbit determination. Both a kinematical orbit determination approach with least squares estimation on the basis of Gauss Markoff

model and reduced-dynamic orbit determination approach with Kalman filter estimation algorithms are investigated by performing variations in the algorithms.

This thesis is composed of four chapters. In Chapter 2, starting from the basic problem of orbit determination, the fundamentals of orbit determination, orbit determination strategies, the reference systems used during orbit determination, the force model and variational equations of motion used for orbit propagation have been explained. The GPS system and pseudorange observables have been introduced. Numerical integration and parameter estimation methodologies used for orbit determination throughout the study have been set up.

In Chapter 3, performed case studies using Bilsat-1 pseudorange observables have been presented. Orbit propagation with two different geopotential models, EGM-96 and EIGEN-CG03C, effect of the degree and order of spherical harmonics used, kinematical orbit determination using precise, rapid and ultra rapid ephemerides, reduced dynamic orbit determination using different state transition implementations and various integration step sizes have been investigated.

In Chapter 4, the results obtained from the assessments have been evaluated and recommendations for further studies have been noted.

CHAPTER 2

ORBIT DETERMINATION OF SMALL SATELLITES

2.1. ORBIT DETERMINATION PROBLEM

Artificial satellites are man made spacecraft sent to space for so many various reasons. The first man made spacecraft being sent to space was in 1957 with the launch of Sputnik I by the Soviet Union. Misra and Enge (2001) mentions an important benefit of both the United States and Soviet Union allocating vast resources to the space race over the next ten years after the first launch as the potential for space based communication, navigation and surveillance systems being recognized and realized quickly.

It would be so easy for a satellite to become useless if locating it and establishing communication with it were not possible. (Montenbruck and Gill, 2000) Therefore, determination of the satellites' orbits is of vital importance for operations.

From the point of artificial satellites, orbit determination problem may be defined as the problem of estimating the parameters defining the state of an orbiting spacecraft consisting of the position and the velocity components at a specific time.

2.2. ORBIT DETERMINATION STRATEGIES

In astrodynamics, orbit determination refers to deriving orbital parameters from observations. (Seeber, 2003) Even though we are now dealing with the orbits of the artificial satellites, satellite orbits have been subject to investigation far before the first spacecraft was launched in 1957. Orbital motion was of interest centuries before

the artificial satellites were invented as the Moon has always been of interest as the natural satellite of the Earth.

Three approaches of orbit determination, which come along as the main methods of solution, may be referred as the dynamic, kinematical and reduced dynamic (hybrid dynamic and kinematical) strategies.

In the dynamic orbit determination approach, mathematical models of the forces acting on the satellite and mathematical models of the satellite's physical properties (altogether usually referred to as dynamic models) are used to compute a model description of the satellite's acceleration over time via the constraints of Newton's second law of motion. Double integration of this model using a nominal spacecraft state vector produces a nominal trajectory − thus developing the equations of motion of the satellite. A model trajectory is then estimated by selecting the satellite state that best fits in a least-squares sense) the pre-processed (un-differenced or differenced) GPS tracking measurements. (Bisnath, 2004; Karslıoğlu, 2004)

In the kinematical orbit determination approach, the dynamics of the satellite (the forces acting on the satellite and other physical properties of the satellite and its environment) are not considered as the major contribution to the problem. The observations and their precision are of more importance for the solution. As far as the measurement model is well defined and the error sources are eliminated, approach results with better performance.

Kinematical positioning requires no a priori knowledge of the spacecraft motion and can thus be applied to a wide range of mission scenarios. However, kinematical methods are particularly sensitive to erroneous measurements, unfavorable viewing geometry and outages, which notably restricts their value in practice. (Motenbruck et al, 2005)

Both strategies have their own weaknesses. Dynamic orbit determination may lead to erroneous results, as perfect modeling of all the forces is not possible all the time.

More detailed the dynamic model is developed, more complicated it becomes for computing and complication in computation always results in cost of time. On the other hand, the kinematical approach behaves as transparent as it could be for the observation errors.

Establishment of a hybrid approach therefore arises in order to be able to account for an optimal solution. Obviously, the search for an optimal solution opens the most fertile area of investigation as the requirements and the definition of the most adequate solution is variable depending on the application areas and priorities.

Satellite orbit determination in such a hybrid approach has two distinct procedures as described by Feng and Zhou (2002). Orbit integration and orbit improvement. Orbit integration yields a nominal orbit trajectory, while orbit improvement estimates the epoch state with all the measurements collected over the data arc in a batch estimation manner.

2.3. TIME AND REFERENCE SYSTEMS

2.3.1. Reference Systems and Reference Frames

Position of any object is defined bounded to a reference system. Reference systems are introduced in order to model geodetic observations as a function of unknown parameters of interest. (Torge, 2001) Appropriate, well defined and reproducible reference coordinate systems are essential for the description of satellite motion, the modeling of observables, and the representation and interpretation of results. The increasing accuracy of many satellite observation techniques requires a corresponding increase in the accuracy of the reference systems. (Seeber, 2003)

A reference system consists of the adopted coordinate system and, in addition, of a set of constants, models and parameters, that are required in order to achieve a certain degree of generality or idealization. Since positioning and navigation are

global activities, nowadays, it is important that the same set definitions is used everywhere. Thus, internationally adopted conventions are necessary.

A reference frame contains all elements required for the materialization of a reference system in real world. In the case of space fixed or celestial frames, it is essentially an adopted catalogue of celestial objects such as stars or quasars, in the case of a terrestrial frame it is the catalogue of coordinates of terrestrial points (stations, observatories) as well as of their velocities. The catalogues are chosen to be consistent with the conventions of the corresponding reference system. (Rummel and Peters, 2001)

The International Earth Rotation Service (IERS) is the organization, which provides and maintains the conventional celestial and terrestrial reference frames, which are the realizations of the reference systems suggested by the International Astronomical Union (IAU) and International Union of Geodesy and Geophysics (IUGG). (Torge, 2001)

An inertial frame is a reference frame in which Newton’s laws of motion apply. It is a non-accelerating frame, which may be in uniform linear motion. A space-fixed, inertial reference system (CIS) for the description of satellite motion is where the Newton's laws of motion are valid.

A Terrestrial Reference System is a spatial reference system co-rotating with the Earth in its diurnal motion in space. In such a system, positions of points anchored on the Earth solid surface have coordinates, which undergo only small variations with time, due to geophysical effects (tectonic or tidal deformations). A Terrestrial Reference Frame is a set of physical points with precisely determined coordinates in a specific coordinate system attached to a Terrestrial Reference System. Such a Terrestrial Reference Frame is said to be a realization of the Terrestrial Reference Frame System.

2.3.2. Transformation Between Celestial and Terrestrial Reference Frames

Each of the reference systems takes an important role in positioning and navigation by space geodetic methods. However, only if we know how to transform one into the other they become operational. Under the assumption of equal scale along each axis and in each of the coordinate systems considered here, transformation from one system into the other consists of a shift of origin from one system to the other system followed by a rotation between base vectors. (Rummel and Peters, 2001)

The transformation from the terrestrial reference frame to the celestial reference frame may be carried out by taking the precession, nutation, polar motion and earth rotation into account. The transformation may be represented by rotation matrices for each effect considered. The main relation between two frames is

$$\mathbf{X}_C = \mathbf{R}_3(\zeta_A)\mathbf{R}_2(-\Theta_A)\mathbf{R}_3(Z_A)\mathbf{R}_1(-\varepsilon_0)\mathbf{R}_3(\Delta\Psi)\mathbf{R}_1(\varepsilon_0+\Delta\varepsilon)\mathbf{R}_3(-\Theta_0)\mathbf{R}_1(y_p)\mathbf{R}_2(x_p)\mathbf{X}_T \tag{2.1}$$

where the rotations to be carried out are

$\mathbf{R}_3(\zeta_A)\mathbf{R}_2(-\Theta_A)\mathbf{R}_3(Z_A)$ representing precession

$\mathbf{R}_1(-\varepsilon_0)\mathbf{R}_3(\Delta\Psi)\mathbf{R}_1(\varepsilon_0+\Delta\varepsilon)$ representing nutation

$\mathbf{R}_3(-\Theta_0)$ representing Greenwich Apparent Sidereal Time

$\mathbf{R}_1(y_p)\mathbf{R}_2(x_p)$ representing the components of polar motion.

Transformation in the opposite direction from the celestial reference frame to the terrestrial reference frame may be achieved by

$$\mathbf{X}_T = \mathbf{R}_1(y_p)\mathbf{R}_2(x_p)\mathbf{R}_3(-\Theta_0)\mathbf{R}_1(-\varepsilon_0)\mathbf{R}_3(\Delta\Psi)\mathbf{R}_1(\varepsilon_0+\Delta\varepsilon)\mathbf{R}_3(\zeta_A)\mathbf{R}_2(-\Theta_A)\mathbf{R}_3(Z_A)\mathbf{X}_C \tag{2.2}$$

2.3.3. Time Systems

In general, there are three different time systems that are used in space geodesy which are dynamical, sidereal and atomic time systems.

All these time scales are based on the observation of uniform and repetitive astronomical or physical phenomena. The time interval between two consecutive phenomena forms the scale measure of the particular time scale. A certain multiple or fraction of the scale measure is called a time unit. In general, the second (s) is used as the basic time unit. Larger time units such as days or years are derived from the second.

Within the time scale, a starting point or origin has to be fixed. This may be achieved through a certain astronomical event, such as the particular position of a star or the meridian transit of a particular celestial object. The instant of the occurrence of some phenomena or observations can be related to a certain reading of the particular time scale, and gives the datation of the event. In astronomy, such an event is called the epoch of the observation. In satellite geodesy the datation of an event is often called time-tag when the instant of transmission or reception of a signal is considered. (Seeber, 2003)

Dynamical time is required for the description of the motion of bodies in a particular reference frame and according to a particular gravitational theory. For satellite orbit computations it is common to use Terrestrial Dynamical Time, which represents a uniform time scale for motion within the earth's gravity field and which has the same rate as that of an atomic clock on the earth, and is in fact defined by that rate. (Misra and Enge, 2001) This time system is also called the Ephemeris Time or Terrestrial Time. Dynamical time is used as the independent variable in the equations of motion, although Barycentric Dynamical time is used for solar system applications. Both were related to International Atomic Time (TAI) at a specified epoch. (Tapley et al., 2004)

The diurnal motion of the earth provides a natural measure for time. Corresponding time systems are introduced in order to relate earth based observations to a space fixed system, Sidereal and Universal (Solar) Time. Hereby, two periodic motions of the Earth play a role. The diurnal rotation of the earth about its polar axis and the annual revolution of the earth around the sun. (Torge, 2001)

Sidereal time and universal time are directly related to the rotation of the Earth, and they are thus equivalent time scales. Sidereal time equals the hour angle of the vernal equinox and consequently depends on the geographical longitude of the particular observation station. The local Apparent Sidereal Time (LAST) referred to the true vernal equinox is the local hour angle of the true vernal equinox. For Greenwich, we obtain the Greenwich Apparent Sidereal Time.

The vernal equinox is subject to nutation in longitude. Removing the nutation term, we obtain the Local mean sidereal time (LMST), and Greenwich Mean Sidereal Time (GMST) respectively as the local hour angle of the mean vernal equinox and the Greenwich hour angle of the mean vernal equinox. (Seeber, 2003)

All civilian time keeping is based on the motion of the sun. Instead of referencing to the vernal equinox, referencing to the sun leads us to the sidereal day, which is the time interval between two successive meridian passes of the sun. This solar day does not coincide with the revolution of the earth around its axis and it is more than a revolution due to the Earth's rotation around the sun once a year.

A uniform time scale of high accuracy is provided by the International Atomic Time. (Temps Atomique International: TAI) It corresponds to the definition of the Standard International second, which has been made approximately equal to the second of the formerly used ephemeris time. The origin of TAI has been chosen so that its epoch (January 1, 1958, 0 h) coincided with the corresponding epoch of Universal Time. (Torge, 2001) TAI is a time scale based on cesium atomic clocks operated by numerous international agencies. In principle, by averaging over numerous atomic clocks, stochastic variations can be diminished and TAI will be a close

approximation of a uniform time scale. (Tapley et al., 2004) The fundamental time scale for all the earth's time keeping is TAI. It is determined with the analyses by the Bureau International des Poids et Measures (BIPM), of the data from atomic clocks all around the world.

2.4. FORCE MODEL

2.4.1. Geopotential and Unperturbed Keplerian Motion of a Satellite

In the framework of Newtonian physics the motion of a satellite under the influence of a force $\mathbf{F}$

$$\mathbf{F} = m\mathbf{a} = m\frac{d^2 s}{dt^2} \tag{2.3}$$

is described by the differential equation

$$\ddot{\mathbf{r}} = \frac{d^2 \mathbf{s}}{dt^2} = \mathbf{F}(t, \mathbf{r}, \mathbf{v}) / m \tag{2.4}$$

where r and v are the position and the velocity of the satellite in a non-rotating geocentric coordinate system, and m denotes the satellite's mass. The elliptic satellite orbits with fixed orbital planes for the special case of a radially symmetric force

$$\mathbf{F} = -m\frac{GM_{\oplus}}{r^2}\mathbf{e}_{\mathbf{r}} \tag{2.5}$$

which decreases with the second power of the distance. Here $\mathbf{e}_{\mathbf{r}}$ denotes the normalized position vector of the satellite pointing in radial direction. This simple inverse-square law describes the gravitational attraction of a point like mass, and can also be shown to be true for extended bodies, provided that they are built up of

concentric shells of constant density. Since this is a basic model for the structure of the earth, Keplerian orbits provide a reasonable first approximation of satellite motion. (Montenbruck and Gill, 2000)

2.4.2. Perturbed Satellite Motion

Unperturbed Keplerian motion assumes that the total mass of the Earth is concentrated in the center of the coordinate system, and the gravitational law therefore be used to calculate the acceleration felt by a satellite at **r**. (Montenbruck and Gill, 2000)

In reality a certain number of additional forces act on the near-Earth satellite, which are called perturbing forces. The satellite experiences additional accelerations because of these forces, which can be combined into a resulting perturbing vector.

Perturbing forces are in particular responsible for the accelerations due to; non-spherically and inhomogeneous mass distribution of the Earth, other celestial bodies (Sun, Moon and other planets), earth tides and oceanic tides, atmospheric drag, direct and earth reflected solar radiation pressure. (Seeber, 2003)

Then the extended equation of motion comprising central body acceleration and all other perturbing accelerations in an earth fixed reference frame is

$$\ddot{\mathbf{r}} = -GM\frac{\mathbf{r}}{r^3} + \mathbf{f}(t, \mathbf{r}, \dot{\mathbf{r}}, q_1, q_2, ..., q_d) + \mathbf{a}_{centr} + \mathbf{a}_{cor} + \mathbf{a}_{rot} \tag{2.6}$$

where

$\ddot{\mathbf{r}}$	is the acceleration vector of the satellite,
$\mathbf{r}$	the position vector of the satellite,
$\dot{\mathbf{r}}$	the velocity vector of the satellite,
q1, … , qd	dynamical parameters that define the satellite force model,

GM the product of the gravity constant, G and the mass of the earth, M,

$-GM\frac{\mathbf{r}}{r^3}$ the gravity acceleration due to central body of the earth,

$\mathbf{f}$ perturbing accelerations acting on the satellite as a function of the spacecraft state and time and dynamical orbit parameters,

t dynamic time (TT),

$\mathbf{a}_{centr}$ centrifugal acceleration due to the rotational motion of the earth fixed frame,

$\mathbf{a}_{cor}$ coriolis acceleration due to the rotational motion of the earth fixed frame and the translational motion of the satellite, and

$\mathbf{a}_{rot}$ the rotational or gyro acceleration due to the non-uniform motion of the earth fixed frame (variations in the angular velocity of the earth). (Karslıoğlu, 2004)

2.4.3. Spherical Harmonics

For the discussion of a more realistic model, it is convenient to use an equivalent representation for acceleration which involves the gradient of the corresponding gravity potential U. (Montenbruck and Gill, 2000)

$$\ddot{\mathbf{r}} = \nabla U \qquad \text{with} \quad U = GM\frac{1}{r} \tag{2.7}$$

For more detailed investigations of the relationship between Earth's anomalous gravitational potential and perturbations of the satellite orbit, it is helpful to use a series expansion with spherical harmonics for the potential, well known from physical geodesy. (Seeber, 2003)

$$U(r,\lambda,\phi) = \frac{GM_{Earth}}{a} \sum_{n=0}^{Max} \sum_{m=0}^{n} \{A_{nm}\ V_{nm} + B_{nm}\ W_{nm}\} \tag{2.8}$$

$$V_{nm} = \left(\frac{a}{r}\right)^{n+1} P_{nm}(\sin\phi)\cos m\lambda\ ,\ W_{nm} = \left(\frac{a}{r}\right)^{n+1} P_{nm}(\sin\phi)\sin m\lambda \tag{2.9}$$

$$x_i = [x, y, z]_i = r\ [\cos\phi\cos\lambda,\ \cos\phi\sin\lambda,\ \sin\phi]_i\ ,\ \ r = |x_i|. \tag{2.10}$$

$$\begin{aligned}
&V_{0,0} = \left(\frac{a}{r}\right)\ ,\ W_{0,0} = 0\ ,\\
&V_{m,m} = (2m-1)\left\{\left(\frac{ax}{r^2}\right)V_{m-1,m-1} - \left(\frac{ay}{r^2}\right)W_{m-1,m-1}\right\}\ ,\\
&W_{m,m} = (2m-1)\left\{\left(\frac{ax}{r^2}\right)W_{m-1,m-1} + \left(\frac{ay}{r^2}\right)V_{m-1,m-1}\right\}\ ,\\
&V_{m+1,m} = (2m+1)\left(\frac{az}{r^2}\right)V_{m,m}\ ,\ W_{m+1,m} = (2m+1)\left(\frac{az}{r^2}\right)W_{m,m}\ ,\\
&V_{n,m} = \left(\frac{2n-1}{n-m}\right)\left(\frac{az}{r^2}\right)V_{n-1,m} - \left(\frac{n+m-1}{n-m}\right)\left(\frac{a^2}{r^2}\right)V_{n-2,m}\ ,\\
&W_{n,m} = \left(\frac{2n-1}{n-m}\right)\left(\frac{az}{r^2}\right)W_{n-1,m} - \left(\frac{n+m-1}{n-m}\right)\left(\frac{a^2}{r^2}\right)W_{n-2,m}\ .
\end{aligned} \tag{2.11}$$

and we finally derive the accelerations due to the non-spherically and inhomogeneous mass distribution of the Earth from

$$\begin{aligned}
a_x &= -\frac{GM_{Earth}}{a^2} A_{n0}\ V_{n+1,1} \quad \text{for } m = 0\ ,\\
&= \frac{GM_{Earth}}{2a^2}\{-A_{nm}\ V_{n+1,m+1} - B_{nm}\ W_{n+1,m+1}\} \quad \text{for } m > 0\\
&+ \frac{GM_{Earth}}{2a^2}\ \frac{(n-m+2)!}{(n-m)!}\{A_{nm}\ V_{n+1,m-1} + B_{nm}\ W_{n+1,m-1}\},
\end{aligned} \tag{2.12}$$

$$
\begin{aligned}
a_y &= -\frac{GM_{Earth}}{a^2} A_{n0}\, W_{n+1,1} \quad \text{for } m = 0\ , \\
&= \frac{GM_{Earth}}{2a^2} \left\{ -A_{nm}\, W_{n+1,m+1} + B_{nm}\, V_{n+1,m+1} \right\} \quad \text{for } m > 0 \\
&+ \frac{Gm_{Earth}}{2a^2} \frac{(n-m+2)!}{(n-m)!} \left\{ -A_{nm}\, W_{n+1,m-1} + B_{nm}\, V_{n+1,m-1} \right\},
\end{aligned}
\tag{2.13}
$$

$$
a_z = \frac{GM_{Earth}}{2a^2} (n-m+1) \left\{ -A_{nm}\, V_{n+1,m} - B_{nm}\, W_{n+1,m} \right\}. \tag{2.14}
$$

2.4.4. Atmospheric Drag

Atmospheric forces represent the largest non-gravitational perturbations acting on the satellites. However, accurate modeling of aerodynamic forces is difficult. Firstly, the physical properties of the atmosphere, in this case especially the density of the upper atmosphere, are not known very accurately. Secondly, the modeling of these forces requires detailed knowledge of the interaction of neutral gas, as well as charged particles, with the different spacecraft surfaces. Finally, the varying attitude of non-spherical satellites with respect to the atmospheric particle flux has to be taken into account. (Montenbruck and Gill, 2000)

The aerodynamic forces acting on the surface of the spacecraft depend on;

- the geometry of the satellite,
- the velocity of the satellite,
- the orientation of the satellite with respect to the flow, and
- the density, temperature and composition of the atmospheric gas.

The appropriate mathematical modeling of the resulting forces turns out to be a rather complicated problem. (Seeber, 2003) The acceleration of a spherical satellite due to atmospheric drag is given by

$$\ddot{\mathbf{r}}_D = -\frac{1}{2} C_D \frac{A}{m} \rho(\mathbf{r}, t) v_r{}^2 \mathbf{e}_v \tag{2.15}$$

where

ρ	is the atmospheric density at the position of the satellite,
v	is the velocity of the satellite relative to the atmosphere,
A	is the satellite reference cross-sectional area
C_D	is the atmospheric drag coefficient
m	is the satellite's mass

Two important variables here are the drag coefficient and atmospheric density at satellite's position. The drag coefficient depends on the interaction of the atmospheric constituents with the satellite surface. The a-priori knowledge of the drag coefficient is not very good, because it depends in a complex way on the spacecraft surface material, the chemical constituents of the atmosphere, the molecular weight and temperature of the impinging particles. Therefore, if possible, the drag coefficient is estimated during the orbit determination process. (Montenbruck and Gill, 2000) For a spherical satellite, the atmospheric density coefficient is approximated as 2. For complicated surfaces like a cylinder, a cone or a plane, it becomes larger. (Seeber, 2003) Determining the atmospheric density is the other challenging task to be accomplished as it includes modeling the dynamics of the Earth's atmosphere.

2.4.4.1. Upper Atmosphere and Atmospheric Density Models

The upper atmosphere is a medium composed of neutral and charged particles, which interact mutually and are subjected to the action of external forcing of solar origin and constrained by the action of gravitational, electric and magnetic fields. To model this medium is to find a satisfactory time description of the behavior of its constituent particles in a chosen space range. Modeling is necessary because it is not feasible to observe the medium structure and dynamics at all places and at all times.

It was during the 60's that thermospheric models received considerable emphasis with the work by Jacchia (1964) who standardized the types of atmospheric variations and ionospheric model development took place with geophysical research purposes. During the 70's upper atmosphere modeling got a definite place in space research with thermosphere modeling based on a spherical harmonics development for each neutral constituent parameter, and ionosphere modeling, which was in part dedicated to communication objectives but started looking at the aim of properly reproducing the behavior of charged particles. (Zamlutti, 1998)

A number of density models are in use today. These include Harris-Priester, Jacchia 1971, Jacchia-Roberts, Jacchia-Linnebery, Jacchia-Gill, Jacchia 1977, CIRA (Cospar International Reference Atmosphere) 1972, CIRA 1986, Hedin, MSIS (Mass Spectrometer and Incoherent Scatter) etc.

2.4.4.2. Harris-Priester Atmospheric Density Model

The Harris-Priester model is based on the properties of the upper atmosphere as determined from the solution of the heat conduction equation under quasi-hydrostatic conditions. While neglecting the explicit dependence of semi-annual and seasonal latitude variations it has been extended to consider the diurnal density bulge. The antapex and apex density at a given latitude h is computed through the exponential interpolation between tabulated minimum and maximum density values.

In addition to its computational simplicity, the benefit of Harris-Priester density model is that it can easily be tailored or extended to other altitude regimes or to other solar flux conditions. (Montenbruck and Gill, 2000)

2.5. VARIATIONAL EQUATIONS

The variational equations of dynamical systems are obtained by linearizing the equations of motion around a particular solution. As with the treatment of the perturbed satellite motion, one may not however, obtain an analytical solution any

more in this case but has to solve a special set of differential equations -the variational equations- by numerical methods. (Montenbruck and Gill, 2000) Numerical solutions are distinguished by their simplicity and universal applicability when compared with analytical methods. The basic idea is that the equations of motion including all perturbations, is integrated stepwise. Aside from the increased accuracy that may be obtained by accounting for perturbations, the concept of the variational equations offers the advantage that it is not limited to the computation of the state transition matrix, but may also be extended to the treatment of partial derivatives with respect to force model parameters. (Seeber, 2003; Montenbruck and Gill, 2000)

2.5.1. State Transition Matrix and Sensitivity Matrix

The partial derivatives of the current state vector with respect to the initial state vector are required for differential correction. These partial derivatives, namely the state transition matrix may be obtained by integrating the variational equations.

The differential equation, which describes the change of the state transition matrix with time, follows from the equation of motion of the satellite. The differential equation of the sensitivity matrix which gives the partial derivatives of the state vector with respect to the force model parameters may be obtained in an analogous way. By combining the differential equations for the state transition matrix and the sensitivity matrix, the following form of the variational equations is obtained.

$$\frac{d}{dt}(\mathbf{\Phi},\mathbf{S}) = \begin{bmatrix} 0_{3x3} & 1_{3x3} \\ \dfrac{\partial \mathbf{a}}{\partial \mathbf{r}} & \dfrac{\partial \mathbf{a}}{\partial \mathbf{v}} \end{bmatrix}_{6x6} \cdot (\mathbf{\Phi},\mathbf{S}) + \begin{bmatrix} 0_{3x6} & 0_{3xn_p} \\ 0_{3x6} & \dfrac{\partial \mathbf{a}}{\partial \mathbf{p}} \end{bmatrix}_{6x(6+n_p)} \tag{2.16}$$

where

$\frac{\partial \mathbf{a}}{\partial \mathbf{r}}$ represents the partial derivatives of acceleration with respect to position of the satellite

$\frac{\partial \mathbf{a}}{\partial \mathbf{v}}$ represents the partial derivatives of acceleration with respect to the velocity of the satellite

$\frac{\partial \mathbf{a}}{\partial \mathbf{p}}$ represents the partial derivatives of acceleration with respect to the force model parameters

The variational equations are integrated simultaneously with the state vector. Otherwise, the position and velocity of the satellite, which are required to evaluate the acceleration partials on the right side of the variational equations, would be unknown. The combined integration of the state vector y, the state transition matrix $\mathbf{\Phi}$, and the sensitivity matrix **S**, therefore requires the solution of (7 + np) six dimensional first order differential equations. (Montenbruck and Gill, 2000)

2.5.2. Partial Derivatives of Geopotential

The variational equations depend on the partial derivatives of acceleration with respect to the state and model parameters. The most important part of the variational equations arises from the geopotential. The partial derivatives of acceleration due to geopotential with respect to position and velocity of the satellite in an earth fixed reference frame are given by;

for ($m = 0$)

$$\frac{\partial \ddot{x}_{nm}}{\partial x} = \frac{GM}{R^3} \cdot \frac{1}{2} \cdot \left\{ \left(+ C_{n0} V_{n+2,2} \right) + \frac{(n+2)!}{n!} \cdot \left(+ C_{n0} V_{n+2,0} \right) \right\} \tag{2.17}$$

$$\frac{\partial \ddot{x}_{nm}}{\partial y} = \frac{GM}{R^3} \cdot \frac{1}{2} \cdot \left\{ \left(+ C_{n0} W_{n+2,2} \right) \right\} \tag{2.18}$$

$$\frac{\partial \ddot{x}_{nm}}{\partial z} = \frac{GM}{R^3} \cdot \left\{ (n+1)\left(+ C_{n0} V_{n+2,1}\right)\right\} \tag{2.19}$$

$$\frac{\partial \ddot{y}_{nm}}{\partial z} = \frac{GM}{R^3} \cdot \left\{ (n+1)\left(+ C_{n0} W_{n+2,1}\right)\right\} \tag{2.20}$$

for ($m = 1$)

$$\frac{\partial \ddot{x}_{nm}}{\partial x} = \frac{GM}{R^3} \cdot \frac{1}{4} \cdot \left\{ \left(+ C_{n1} V_{n+2,3} + S_{n1} W_{n+2,3}\right) + \frac{(n+1)!}{(n-1)!} \cdot \left(- C_{n1} V_{n+2,1} - S_{n1} W_{n+2,1}\right)\right\} \tag{2.21}$$

$$\frac{\partial \ddot{x}_{nm}}{\partial y} = \frac{GM}{R^3} \cdot \frac{1}{4} \cdot \left\{ \left(+ C_{n1} W_{n+2,3} - S_{n1} V_{n+2,3}\right) + \frac{(n+1)!}{(n-1)!} \cdot \left(- C_{n1} W_{n+2,1} - S_{n1} V_{n+2,1}\right)\right\} \tag{2.22}$$

for (m>0)

$$\frac{\partial \ddot{x}_{nm}}{\partial z} = \frac{GM}{R^3} \cdot \left\{ \frac{n-m+1}{2}\left(+ C_{nm} V_{n+2,m+1} + S_{nm} W_{n+2,m+1}\right) + \frac{(n-m+3)!}{2(n-m)!} \cdot \left(- C_{nm} V_{n+2,m-1} - S_{nm} W_{n+2,m-1}\right)\right\} \tag{2.23}$$

$$\frac{\partial \ddot{y}_{nm}}{\partial z} = \frac{GM}{R^3} \cdot \left\{ \frac{n-m+1}{2}\left(+ C_{nm} W_{n+2,m+1} - S_{nm} V_{n+2,m+1}\right) + \frac{(n-m+3)!}{2(n-m)!} \cdot \left(+ C_{nm} W_{n+2,m-1} - S_{nm} V_{n+2,m-1}\right)\right\} \tag{2.24}$$

$$\frac{\partial \ddot{z}_{nm}}{\partial z} = \frac{GM}{R^3} \cdot \left\{ \frac{(n-m+2)!}{(n-m)!} \cdot \left(+ C_{nm} V_{n+2,m} + S_{nm} V_{n+2,m}\right)\right\} \tag{2.25}$$

for ($m > 1$)

$$\frac{\partial \ddot{x}_{nm}}{\partial x} = \frac{GM}{R^3} \cdot \frac{1}{4} \cdot \left\{ \left(+ C_{nm} V_{n+2,m+2} + S_{nm} W_{n+2,m+2}\right) + 2\frac{(n-m+2)!}{(n-m)!} \cdot \left(- C_{nm} V_{n+2,m} - S_{n1} W_{n+2,1}\right) + \frac{(n-m+4)!}{(n-m)!} \cdot \left(+ C_{nm} V_{n+2,m-2} + S_{nm} W_{n+2,m-2}\right)\right\} \tag{2.26}$$

$$\frac{\partial \ddot{x}_{nm}}{\partial y} = \frac{GM}{R^3} \cdot \frac{1}{4} \cdot \left\{ \left(+ C_{nm} W_{n+2,m+2} - S_{nm} V_{n+2,m+2} \right) \right.$$

$$\left. + \frac{(n-m+4)!}{(n-m)!} \cdot \left(- C_{nm} W_{n+2,m-2} + S_{nm} W_{n+2,m-2} \right) \right\} \quad (2.27)$$

2.5.3. Partial Derivatives of Atmospheric Drag

Starting from the basic equation in (2.15)

$$\ddot{\mathbf{r}}_D = -\frac{1}{2} C_D \frac{A}{m} \rho(\mathbf{r}, t) v_r{}^2 \mathbf{e}_{\mathbf{v}} \quad (2.28)$$

The partial derivatives of acceleration due to atmospheric drag with respect to the velocity of the satellite is

$$\frac{\partial \ddot{\mathbf{r}}}{\partial v} = -\frac{1}{2} C_D \frac{A}{m} \rho \left(\frac{\mathbf{v_r} \mathbf{v_r^T}}{v_r} + v_r \mathbf{1} \right) \quad (2.29)$$

and the partial derivatives of acceleration due to atmospheric drag with respect to position of the satellite is

$$\frac{\partial \ddot{\mathbf{r}}}{\partial r} = -\frac{1}{2} C_D \frac{A}{m} v_r \mathbf{v_r} \frac{\partial \rho}{\partial r} - \frac{1}{2} C_D \frac{A}{m} \rho \left(\frac{\mathbf{v_r} \mathbf{v_r^T}}{v_r} + v_r \mathbf{1} \right) \frac{\partial \mathbf{v_r}}{\partial \mathbf{r}} \quad (2.30)$$

2.6. NUMERICAL INTEGRATION

2.6.1. Runge-Kutta 4th Order Numerical Integration

The orbit propagation method is one of the most important problems in analyzing and controlling missions, which involves artificial satellites. In practice, the numerical method is the most used one, as the Cowell's method. The Cowell's method consists of integrating the satellite's equations of motion with all

perturbations step by step and it involves straight integration of velocity and acceleration time step. The perturbations can be included in the same time. The acceleration is found by evaluating the forces acting on the spacecraft. (Chiradia et al., 2000)

Starting from initial values $y_0 = y(t_0)$ at time t_0 one may calculate simple approximation of y at some later time $t_0 + h$ from a first order Taylor expansion

$$y(t_0 + h) \approx y_0 + h\dot{y} = y_0 + h\mathbf{f}(t_0, y_0) \tag{2.31}$$

which is known as the Euler's method. Performing a subsequent of Euler steps, approximate values of the solution at distinct times are obtained.

Improved expressions for such an approximation are developed by Carl Runge and Wilhelm Kutta at the end of 19th century.

4th order Runge-Kutta (RK4) algorithm is considered an adequate numerical integrator due to its simplicity, fair accuracy, low truncation error, and low computational burden. It does not need an initialization procedure and the step size is easy to change. The RK4 algorithm is as follows:

$$\begin{aligned}
&y(t_0 + h) \approx y_0 + h\Phi \\
&\Phi = \frac{1}{6}(k_1 + 2k_2 + 2k_3 + k_4) \\
&k_1 = f(t_0, y_0) \\
&k_2 = f(t_0 + h/2, y_0 + hk_1/2) \\
&k_3 = f(t_0 + h/2, y_0 + hk_2/2) \\
&k_4 = f(t_0 + h/2, y_0 + hk_3)
\end{aligned} \tag{2.32}$$

It is initialized by specifying the initial spacecraft state at some epoch. It continues by specifying an integration time step and evaluating the above equations. The variable $f(t, y)$ represents the derivatives of the spacecraft state vector, i.e. velocity and acceleration, on the spacecraft at time t and state y .

2.7. THE GLOBAL POSITIONING SYSTEM (GPS)

2.7.1. GPS Overview

The Global Positioning System (GPS) is a space-based radio navigation system managed and operated by the United States (U.S.) Government. GPS was designed as a dual-use system with the primary purpose of enhancing the effectiveness of U.S. and allied military forces. Two GPS services are provided. The Precise Positioning Service (PPS) is available primarily to the military and other authorized users equipped with PPS receivers. The Standard Positioning Service (SPS) was originally designed to provide civil users with a less accurate positioning capability than PPS through the use of a technique known as Selective Availability (SA). On May 1, 2000, the use of SA has been removed from the system. (Stenbit, 2001)

The fully operational GPS includes 24 or more (28 in March 2000) satellites approximately uniformly dispersed around six circular orbits with four or more satellites each. The orbits are inclined at an angle of 55˚ relative to the equator and are separated from each other by multiples of 60˚ right ascension. The orbits are nongeostationary and approximately circular, with radii of 26,560 km and orbital periods of one-half sidereal day (≈11.967 h). Theoretically, three or more GPS satellites will always be visible from most points on the Earth's surface, and four or more GPS satellites can be used to determine an observer's position anywhere on Earth's surface 24 hours per day. (Grewal, 2001)

The GPS is a one way ranging system. The GPS satellites emit signals -complex modulated radio waves- which propagate through space to receivers on or near

Earth's surface. From the signals it intercepts, a receiver measures the ranges between its antenna and the satellites. (Kleusberg and Teunissen, 1996)

The GPS consists of three major segments: the space segment, the control segment and the user segment. The space segment consists of the satellites; the control segment consists of five monitor stations, a master control station and three ground control stations. The user segment consists of military and civilian users equipped with GPS receivers for various purposes.

The GPS satellites transmit microwave carrier signals at the L1 frequency (1575.42 MHz) and the L2 frequency (1227.60 MHz). The second frequency allows measurement of the ionospheric signal delay using PPS-capable receivers. Each satellite transmits signals on both frequencies. These are the navigation signals (codes), and the navigation and system data (message). The codes are modulated on the carrier frequencies as so-called pseudo random noise (PRN) sequences. Three binary codes are modulated on the L1 or L2 carrier or both. The L1 signal contains both the precise P code and the less precise C/A code. The L2 signal contains only the P code. The navigation data is added to both the C/a and P codes on L1 frequency and depending on the satellite mode also on the L2 frequency. (Seeber, 2003; Montenbruck and Gill, 2000)

2.7.2. GPS Pseudorange Observables

The basic observables of the GPS, which permit us to determine position, velocity and time, are the pseudorange, and the carrier phase. Additional observables that have certain advantages can be generated by combining the basic observables in various ways.

The PRN codes transmitted by a satellite are used to determine the pseudorange – a measure of range between the satellite antenna and the antenna feeding a GPS receiver. A pseudorange from code measurements equals the time shift that is necessary to correlate the incoming code sequence with a code sequence generated in

the GPS receiver, multiplied by the velocity of light. The receiver makes this measurement by replicating the code being generated by the satellite and determining, the time offset between the arrival of a particular transition in the code and that same transition in the code replica. The time offset is simply the time the signal takes to propagate from the satellite to the receiver. The pseudorange is the time offset multiplied by the speed of light. The reason the observable is called pseudorange is that it is biased by the lack of time synchronization between the clock in the GPS satellite governing the generation of the satellite signal and the clock in the GPS receiver governing the generation of the code replica. (Seeber, 2003; Kleusberg and Teunissen, 1996)

The fundamental observation equation for a single pseudorange is;

$$PR_i = \rho + c.\delta t_u = c.\tau_i = ((X_i - X_B)^2 + (Y_i - Y_B)^2 + (Z_i - Z_B)^2)^{1/2} + c.\delta t_u \qquad (2.33)$$

where

ρ	geometrical distance (slant range) between satellite and receiver
X_i	X coordinate component of the satellite's position
Y_i	Y coordinate component of the satellite's position
Y_i	Z coordinate component of the satellite's position
X_B	X coordinate component of the receiver's position
Y_B	Y coordinate component of the receiver's position
Z_b	Z coordinate component of the receiver's position
τ_i	observed signal propagation time between satellite an receiver
δt_u	clock synchronization error between GPS time and receiver clock
c	signal propagation velocity

2.7.3. GPS Error Sources

The observed pseudoranges are affected by several error sources. These include the ionospheric and tropospheric delays, multipath, receiver clock error, satellite clock and ephemeris errors, multipath and receiver noise. We can write the pseudorange observable that relates the measurement and the various biases;

$$PR = \rho + c.(dt - dT) + d_{ion} + d_{trop} + e \tag{2.34}$$

where in addition to the equation 2.33;

d_{ion}	is the ionospheric delay
d_{trop}	is the tropospheric delay
dt, dT	are the offsets of the satellite and receiver clocks from GPS time
e	the multipath, receiver noise, ephemeris errors

The objective in GPS positioning is to mathematically describe all the terms on the right hand side of the equation including the initially unknown receiver coordinates in the geometric range term, so that the sum of terms equals the measurement value on the left hand side. Any error in the description of the terms will result in the derived receiver coordinates. (Kleusberg and Teunissen, 1996)

2.8. PARAMETER ESTIMATION

2.8.1. Least Squares Estimation on the Basis of Gauss Markoff Model

The least squares criterion was first proposed by Gauss (1809) and is commonly used today. The least squares solution selects the estimate of the unknown parameters as the value that minimizes the sum of the squares of the calculated observation residuals. (Tapley et al., 2004) This sensible method of estimating the unknown parameters is given by minimizing the sum of the squares of the deviations of the observations from the estimators of their expected values, which are the functions of the unknown parameters. (Koch, 1999) The sum of the squares of the calculated

observation errors is a logical choice for the performance index. A criterion defined, for example, by the sum of the calculated observation errors could be identically zero with very large observation errors having plus and minus signs that cancel with each other. Whether the observation error is positive or negative, its square will be positive and the performance index can only vanish if each of the observation errors is identically zero. (Tapley et al., 2004)

Let **X** be an n x u matrix of given coefficients, $\boldsymbol{\beta}$ a u x 1 vector of unknown parameters, $\boldsymbol{y}$ an n x 1 random vector of observations and $D(\mathbf{y}) = \sigma^2 \mathbf{P}^{-1}$ the n x n covariance matrix of $\boldsymbol{y}$, where the weight matrix $\boldsymbol{P}$ of the observations $\boldsymbol{y}$ is known and the positive factor σ^2 is unknown. Let $\boldsymbol{X}$ have full column rank, i.e., rank$\boldsymbol{X}$ = u, and let the weight matrix $\boldsymbol{P}$ be positive and definite. Then

$$\boldsymbol{X\beta} = E(\boldsymbol{y}) \tag{2.35}$$

with

$$D(\mathbf{y}) = \sigma^2 \mathbf{P}^{-1} \tag{2.36}$$

is said to be a Gauss-Markoff model with full rank.

One assumes in this model that the expected values of the observations $\boldsymbol{y}$ can be represented by a linear combination of the given coefficients and the unknown parameters. Hence, a linear model is given. The linear relation follows generally after a linearization, from physical or mathematical laws, that is from quantitative statements. (Koch, 1999)

By adding the n x 1 random vectors $\boldsymbol{e}$ of the errors of $\boldsymbol{y}$ one obtains the consistent system

$$\boldsymbol{X\beta} = \boldsymbol{y} + \boldsymbol{e} \tag{2.37}$$

In case of $\boldsymbol{P} = \boldsymbol{I}$, where $\boldsymbol{I}$ is identity matrix, equation 2.36 becomes

$$D(\boldsymbol{y}) = \sigma^2 \boldsymbol{I} \tag{2.38}$$

The best linear unbiased estimator $\hat{\boldsymbol{\beta}}$ of the unknown parameters $\boldsymbol{\beta}$ and its covariance matrix $D(\hat{\boldsymbol{\beta}})$ which possesses minimum trace, is given in the Gauss-Markoff model by

$$\hat{\boldsymbol{\beta}} = (\boldsymbol{X}^T \boldsymbol{X})^{-1} \boldsymbol{X}^T \boldsymbol{y} \tag{2.39}$$

and

$$D(\hat{\boldsymbol{\beta}}) = \sigma^2 (\boldsymbol{X}^T \boldsymbol{X})^{-1} \tag{2.40}$$

2.8.2. Discrete Kalman Filtering

In 1960, R.E. Kalman published his famous paper describing a recursive solution to the discrete-data linear filtering problem. He provided an alternative way of formulating the minimum mean square error filtering problem using state-space methods. Since that time, due in large part to advances in digital computing; the Kalman filter has been the subject of extensive research and application, particularly in the area of autonomous or assisted navigation. (Brown and Hwang, 1997; Bishop and Welch, 2002)

The Kalman filter is a set of mathematical equations that provides an efficient computational (recursive) solution of the least-squares method. The filter is very powerful in several aspects: it supports estimations of past, present, and even future states, and it can do so even when the precise nature of the modeled system is unknown. (Bishop and Welch, 2002)

The two main features of the Kalman formulation and solution of the problem are; vector modeling of the random processes under consideration and recursive processing of the noisy measurement input data.

The Kalman filter addresses the general problem of trying to estimate the state *x* of a discrete-time controlled process that is governed by the linear stochastic difference equation;

$$x_k = Ax_{k-1} + Bu_k + w_{k-1} \tag{2.40}$$

with a measurement z that is;

$$z_k = Hx_k + v_k \tag{2.41}$$

The random variables v_k and w_k represent the process and measurement noise (respectively). They are assumed to be independent (of each other), white, and with normal probability distributions. In practice, the process noise covariance $\boldsymbol{Q}$ and measurement noise covariance $\boldsymbol{R}$ matrices might change with each time step or measurement, however here we assume they are constant.

2.8.2.1 Discrete Extended Kalman Filter

The essential idea of the extended Kalman filter was proposed by Stanley F. Schmidt and it has been called the Kalman Schmidt filter .Extended Kalman Filter is nonlinear Kalman filtering with all jacobian matrices evaluated at the estimated state. The major differences from the conventional Kalman filter equations are;

- integration of the non-linear integrand $\dot{x} = f(x)$ to predict $x_k\ (-)$
- use of the nonlinear function $h_k(x_k\ (-))$ in measurement prediction
- use of jacobian matrix of the dynamic model function $\boldsymbol{f}$ as the dynamic coefficient matrix **F** in the propagation of the covariance matrix, and

- use of jacobian matrix of the measurement function **H** in the covariance correction and Kalman gain equations

The Kalman filter estimates a process by using a form of feedback control. The filter estimates the process state at some time and then obtains feedback in the form of (noisy) measurements. As such, the equations for the Kalman filter fall into two groups; time update equations and measurement update equations. The time update equations are responsible for projecting forward (in time) the current state and error covariance estimates to obtain the a priori estimates for the next time step. The measurement update equations are responsible for the feedback -i.e. for incorporating a new measurement into the a priori estimate to obtain an improved a posteriori estimate. (Bishop and Welch, 2002)

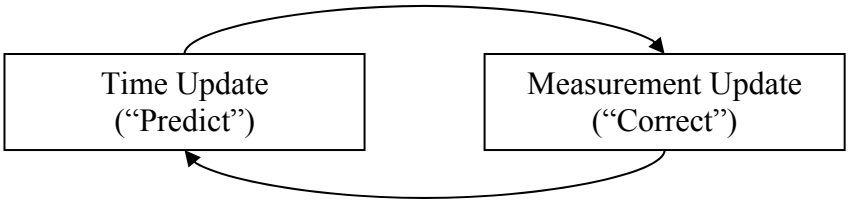

Figure 2.1. Kalman Filter Time and Measurement Update Procedure

The extended Kalman filter time update equations are;

$$x_k^- = x_{k-1}^+ + \int f(x,t)dt \tag{2.42}$$

$$P_k^- = \Phi_k P_{k-1}^+ \Phi_k^T + Q_{k-1} \tag{2.43}$$

The extended Kalman filter measurement update equations are;

$$K_k = P_k^- H_k^T (H_k P_k^- H_k^T + R_k)^{-1} \tag{2.44}$$

$$x_k^+ = x_k^- + K_k \left[z_k - h_k(x_k^-) \right] \tag{2.45}$$

$$P_k^+ = P_k^- - K_k H_k P_k^- \tag{2.46}$$

where

x_k^-	predicted state of current epoch
x_{k-1}^+	estimated state of the previous epoch
P_k^-	predicted state estimate error covariance
P_k^+	corrected state estimate error covariance
K_k	Kalman gain
H_k	measurement sensitivity matrix
R_k	measurement error covariance
Q_k	process noise covariance

CHAPTER 3

ORBIT DETERMINATION FOR BILSAT-1

3.1. BILSAT-1 MISSION OVERVIEW

BILSAT-1 is a 129 kg enhanced microsatellite developed by SSTL with TUBITAK-BILTEN engineers as part of a technology transfer program. The main objective of the mission is remote sensing. The multispectral imager of the satellite has a 26-metre ground sampling distance at 686 km altitude giving a swath width of 55 km and the panchromatic imager of the satellite with 12-metre ground sampling distance gives a 25 km swath width.

The main objective of the mission is remote sensing and as such, the system has been designed around these requirements with a set of subsystems that make the maximum use of the imaging capability installed on board. The attitude determination and control subsystem of BİLSAT-1 features a suite of sensors comprising four sun sensors, four rate sensors, two magnetometers and two star cameras (a GPS receiver is used for position determination). Four reaction wheels, three torque rods, and a gravity gradient boom account for the actuators. (Orlu et al., 2003)

The SSTL SGR-20 model 24 channel GPS receiver is installed on board the satellite, which is produced by Surrey Satellite Technology Ltd.

3.2. ORBIT PREDICTION

As Bilsat-1 is a low earth orbiting artificial satellite, two main important forces; the geopotential and the atmospheric drag acting on satellites orbiting at low altitude have been considered in this study when establishing the equations of motion for orbit propagation.

The translational equation of motion of the spacecraft in an earth fixed geocentric reference frame given in Chapter 2 to with the equation 2.6 which is repeated here in equation 3.1 is considered by taking into account the geopotential and the atmospheric drag as the perturbing accelerations on the spacecraft and corrections due to coriolis and centrifugal forces.

$$\ddot{\mathbf{r}} = -GM\frac{\mathbf{r}}{r^3} + \mathbf{f}(t, \mathbf{r}, \dot{\mathbf{r}}, q_1, q_2, ..., q_d) + \mathbf{a}_{centr} + \mathbf{a}_{cor} + \mathbf{a}_{rot} \tag{3.1}$$

When integrating the equations of motion in an earth fixed geocentric reference frame, so-called apparent forces arise if the equation of motion is formulated with respect to a moving reference system instead of a fixed one. (Seeber, 2003) Accelerations resulting from inertial centrifugal and coriolis forces have been taken into account together with the total acceleration vector during orbit determination of Bilsat-1.

Coriolis and centrifugal accelerations in an earth fixed geocentric reference frame are given by,

$$\mathbf{a}_{cor} = -2m\boldsymbol{\omega} \times \mathbf{v} \tag{3.2}$$

$$\mathbf{a}_{centr} = -m \times \boldsymbol{\omega} \times (\boldsymbol{\omega} \times \mathbf{r}) \tag{3.3}$$

where

$\boldsymbol{\omega}$ is the angular velocity of Earth,

r	is the position vector in the Earth fixed geocentric reference frame
v	is the velocity vector in the Earth fixed geocentric reference frame

3.2.1. Geopotential Models

3.2.1.1 EGM-96 Geopotential Model

The NASA Goddard Space Flight Center (GSFC), the National Imagery and Mapping Agency (NIMA), and the Ohio State University (OSU) have collaborated to develop an improved spherical harmonic model of the Earth's gravitational potential to degree 360. Earth Gravitational Model 1996 (EGM96) incorporates improved surface gravity data, altimeter-derived anomalies from ERS-1 and from the GEOSAT Geodetic Mission (GM), extensive satellite tracking data - including new data from Satellite laser ranging (SLR), the Global Positioning System (GPS), NASA's Tracking and Data Relay Satellite System (TDRSS), the French DORIS system, and the US Navy TRANET Doppler tracking system - as well as direct altimeter ranges from TOPEX/POSEIDON (T/P), ERS-1, and GEOSAT. The final solution blends a low-degree combination model to degree 70, a block-diagonal solution from degree 71 to 359, and a quadrature solution at degree 360. The model was used to compute geoid undulations accurate to better than one meter (with the exception of areas void of dense and accurate surface gravity data) and realize WGS84 as a true three-dimensional reference system. (Lemoine et al., 1998)

3.2.1.2 EIGEN-CG03C Geopotential Model

EIGEN-CG03C is a global mean gravity field model, which is a combination of the GRACE mission (376 days out of February to May/July to December 2003 and February to July 2004), and the CHAMP mission (860 days out of October 2000 to June 2003) data plus altimetric and gravimetric surface data. This model is an upgrade of EIGEN-CG01C, which was based on the same CHAMP and surface data. EIGEN-CG03C is complete to degree/order 360 in terms of spherical harmonic coefficients and resolves wavelengths of 110 km in the geoid and gravity anomaly

fields. The overall accuracy of the full model is estimated to be 30 cm and 8 mgal, respectively, and benefits also from recently issued new gravity anomaly compilations over polar regions. (Förste et al., 2005)

3.2.1.3 Variations in Bilsat-1 Orbit Prediction Due To Geopotential Model

The coefficients of EGM96 and EIGEN-CG03C geopotential models have been alternatively used for the geopotential component of the force model established for this study. Orbit propagation has been performed using both geopotential models and the differences between these two orbit predictions have been calculated for one hour time span.

Figures 3.1, 3.2 and 3.3 show respectively the differences of x, y, and z components of the position of Bilsat-1 calculated for EGM96 and EIGEN-CG03C orbit prediction solutions considering only the J2 term of the spherical harmonics.

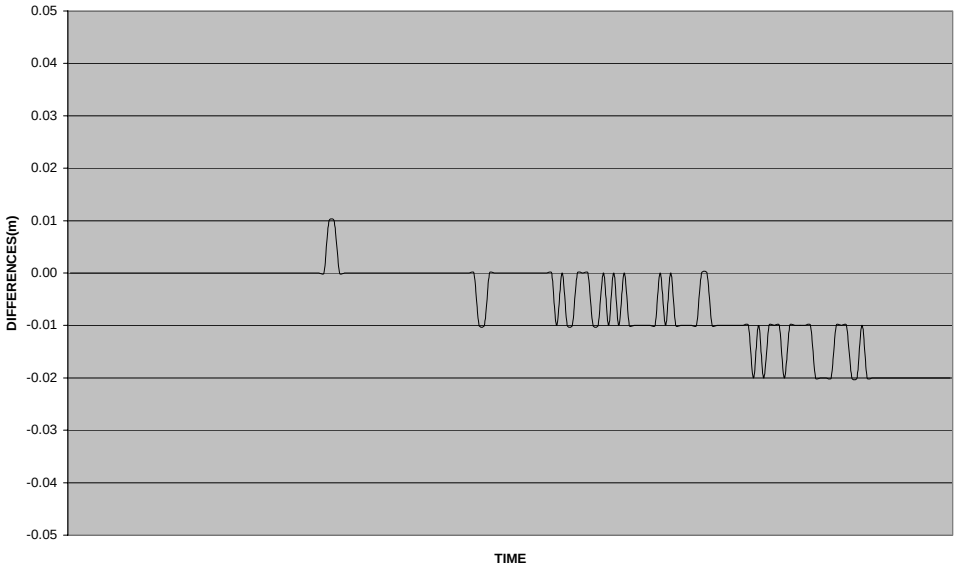

Figure 3.1. Differences of the x component of Bilsat-1 position between EGM96 and EIGEN-CG03C orbit predictions considering J2 term of spherical harmonics.

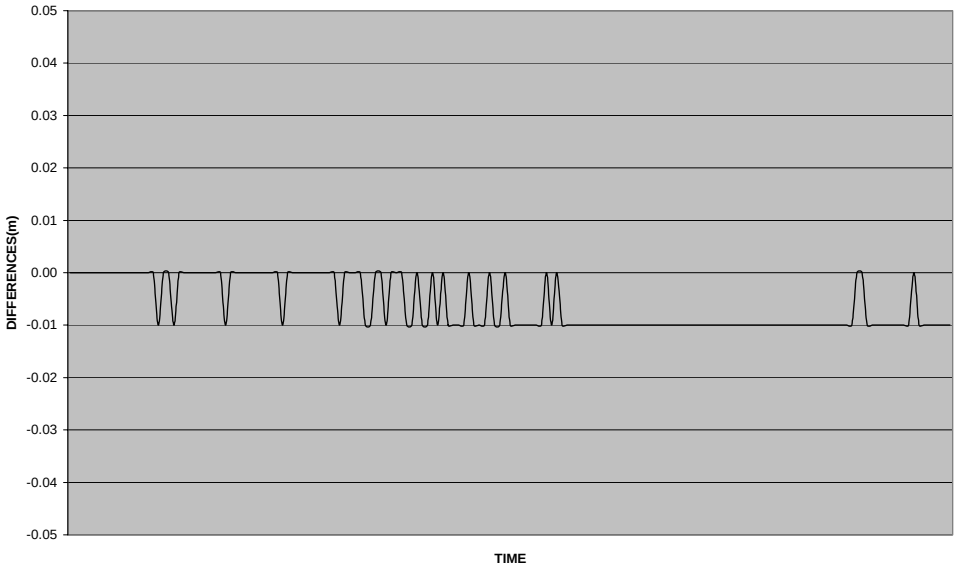

Figure 3.2. Differences of the y component of Bilsat-1 position between EGM96 and EIGEN-CG03C orbit predictions considering J2 term of spherical harmonics.

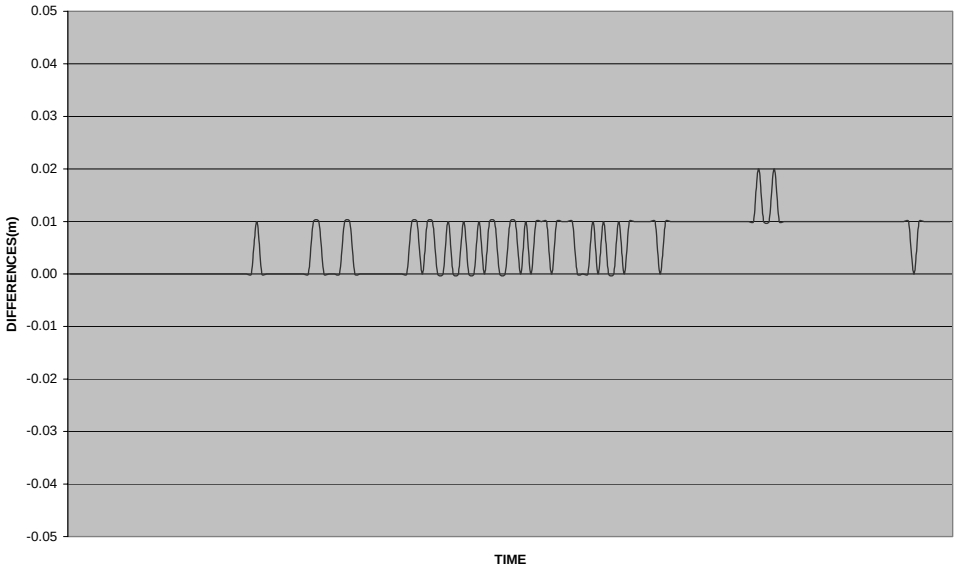

Figure 3.3. Differences of the z component of Bilsat-1 position between EGM96 and EIGEN-CG03C orbit predictions considering J2 term of spherical harmonics.

The corresponding standard deviations for x, y, z and position of Bilsat-1 calculated for EGM96 and EIGEN-CG03C orbit prediction solutions considering only the J2 term of the spherical harmonics are calculated as 7.6 mm, 4.9 mm, 5.2 mm , and 10 mm respectively.

Figures 3.4, 3.5 and 3.6 show respectively the differences of x, y, and z components of the position of Bilsat-1 calculated for EGM96 and EIGEN-CG03C orbit prediction solutions considering the degree and order of the spherical harmonic coefficients up to the order and degree of 10.

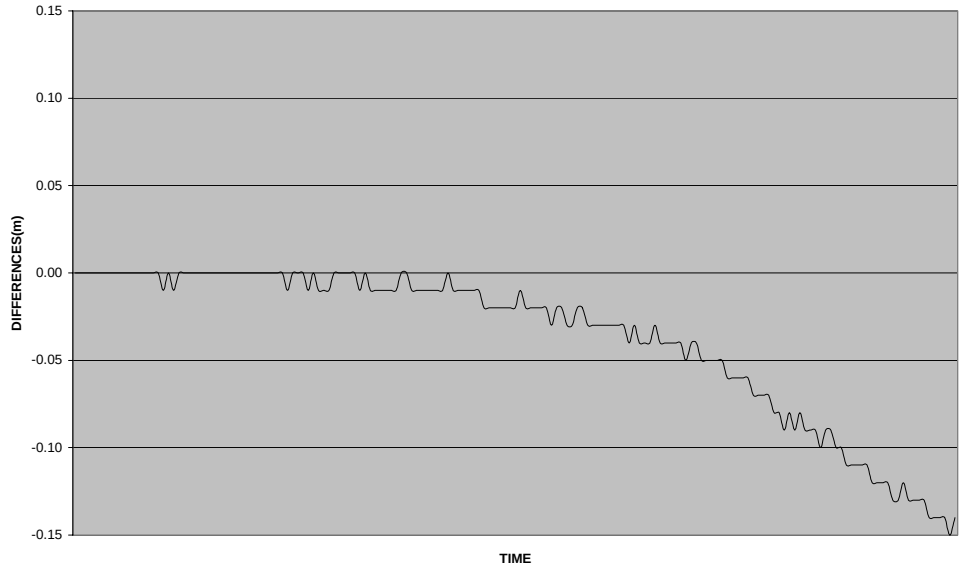

Figure 3.4. Differences of the x component of Bilsat-1 position between EGM96 and EIGEN-CG03C orbit predictions considering the degree and order of the spherical harmonic coefficients up to 10.

The corresponding standard deviations for x, y, z and position of Bilsat-1 calculated for EGM96 and EIGEN-CG03C orbit prediction solutions considering the degree and order of the spherical harmonic coefficients up to 10 are calculated as 4.36 cm, 0.06 cm, 2.71 cm , and 5.17 cm respectively.

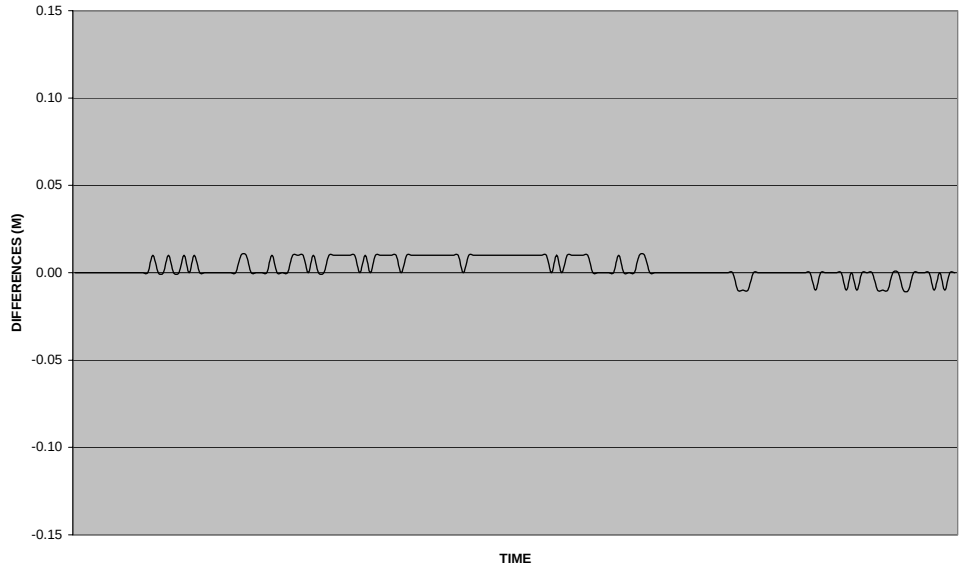

Figure 3.5. Differences of the y component of Bilsat-1 position between EGM96 and EIGEN-CG03C orbit predictions considering the degree and order of the spherical harmonic coefficients up to 10.

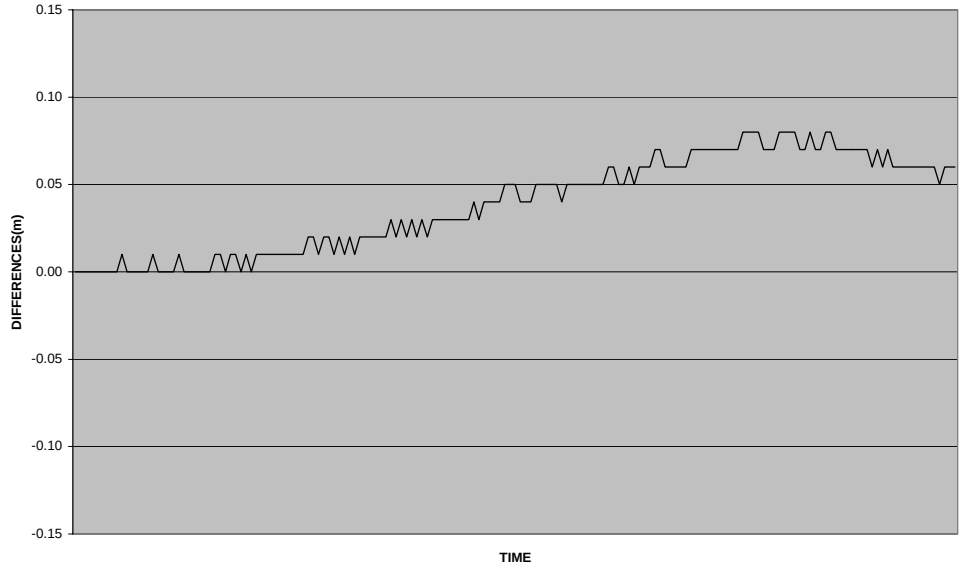

Figure 3.6. Differences of the z component of Bilsat-1 position between EGM96 and EIGEN-CG03C orbit predictions considering the degree and order of the spherical harmonic coefficients up to 10.

Figures 3.7, 3.8 and 3.9 show respectively the differences of x, y, and z components of the position of Bilsat-1 calculated for EGM96 and EIGEN-CG03C orbit prediction solutions considering the degree and order of the spherical harmonic coefficients up to the order and degree of 20.

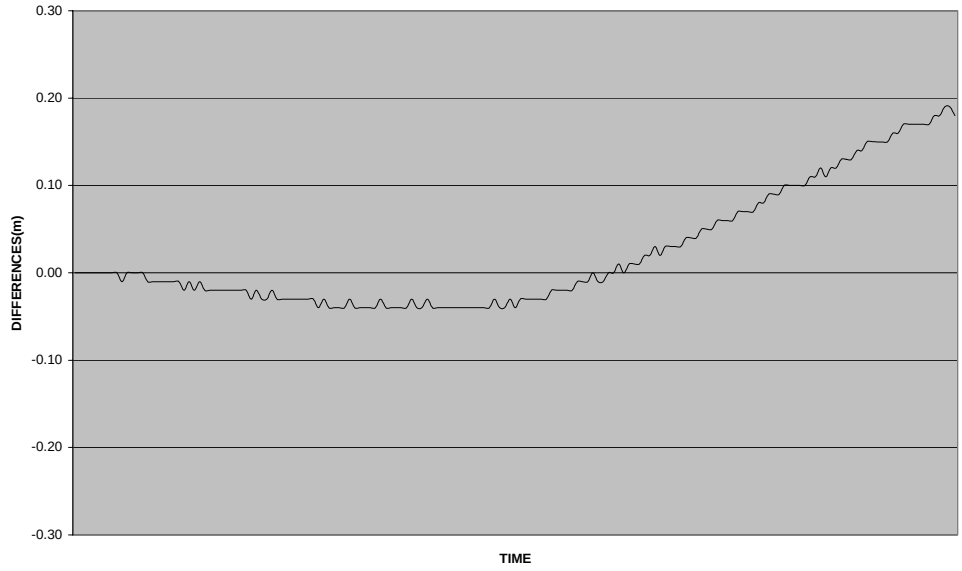

Figure 3.7. Differences of the x component of Bilsat-1 position between EGM96 and EIGEN-CG03C orbit predictions considering the degree and order of the spherical harmonic coefficients up to 20.

The corresponding standard deviations for x, y, z and position of Bilsat-1 calculated for EGM96 and EIGEN-CG03C orbit prediction solutions considering the degree and order of the spherical harmonic coefficients up to 20 are calculated as 6.91 cm, 2.81 cm, 7.97 cm , and 10.91 cm respectively.

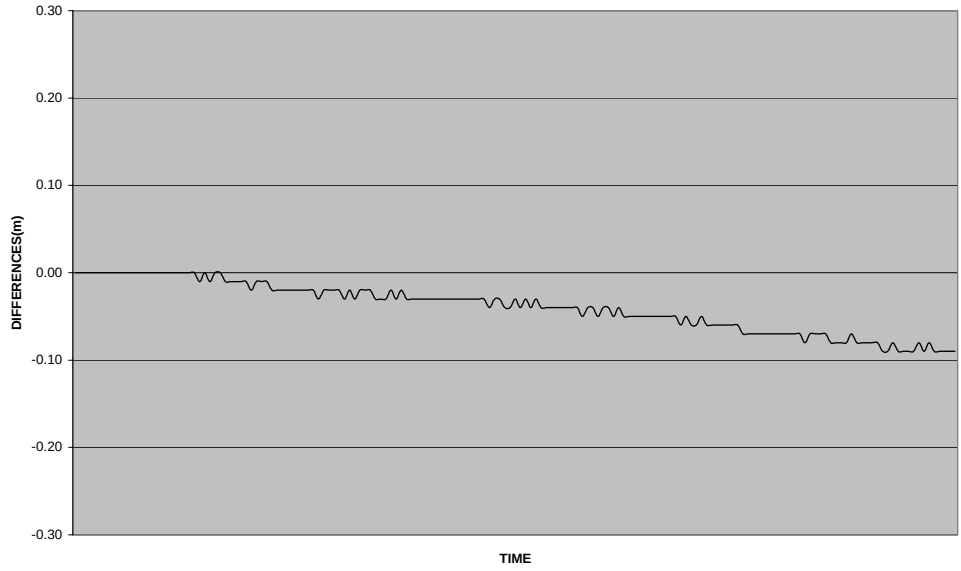

Figure 3.8. Differences of the y component of Bilsat-1 position between EGM96 and EIGEN-CG03C orbit predictions considering the degree and order of the spherical harmonic coefficients up to 20.

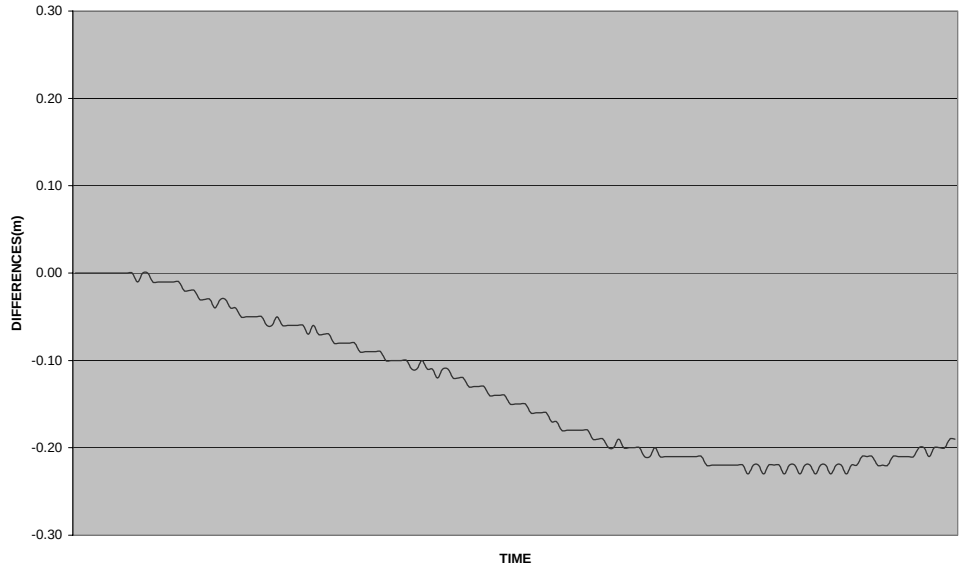

Figure 3.9. Differences of the z component of Bilsat-1 position between EGM96 and EIGEN-CG03C orbit predictions considering the degree and order of the spherical harmonic coefficients up to 20.

Figures 3.10, 3.11 and 3.12 show respectively the differences of x, y, and z components of the position of Bilsat-1 calculated for EGM96 and EIGEN-CG03C orbit prediction solutions considering the degree and order of the spherical harmonic coefficients up to the order and degree of 50.

The corresponding standard deviations for x, y, z and position of Bilsat-1 calculated for EGM96 and EIGEN-CG03C orbit prediction solutions considering the degree and order of the spherical harmonic coefficients up to 50 are calculated as 7.03 cm, 2.23 cm, 10.43 cm , and 12.77 cm respectively.

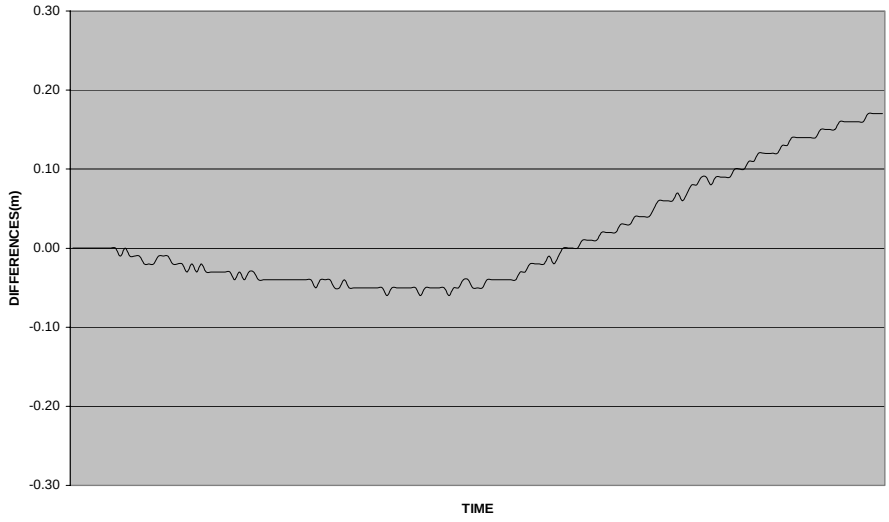

Figure 3.10. Differences of the x component of Bilsat-1 position between EGM96 and EIGEN-CG03C orbit predictions considering the degree and order of the spherical harmonic coefficients up to 50.

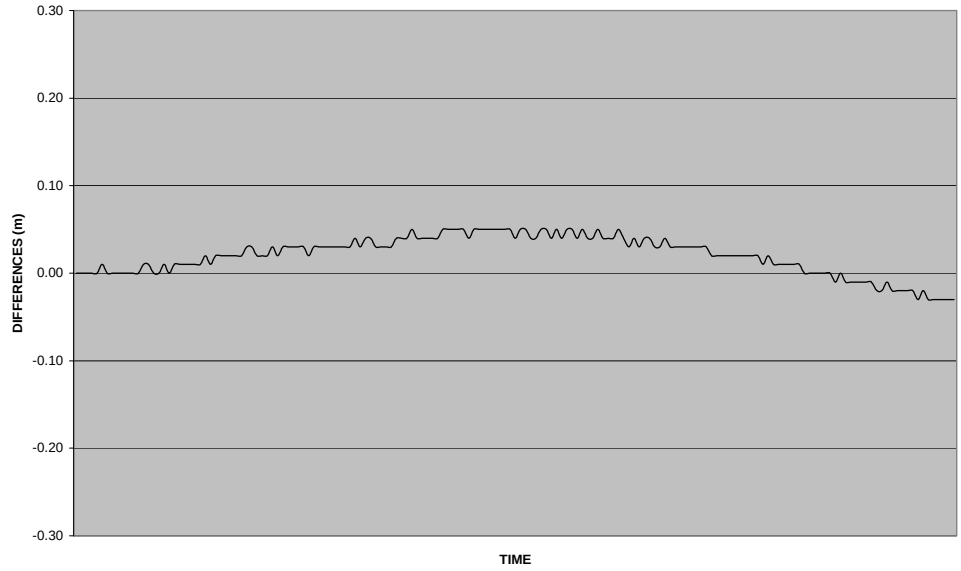

Figure 3.11. Differences of the y component of Bilsat-1 position between EGM96 and EIGEN-CG03C orbit predictions considering the degree and order of the spherical harmonic coefficients up to 50.

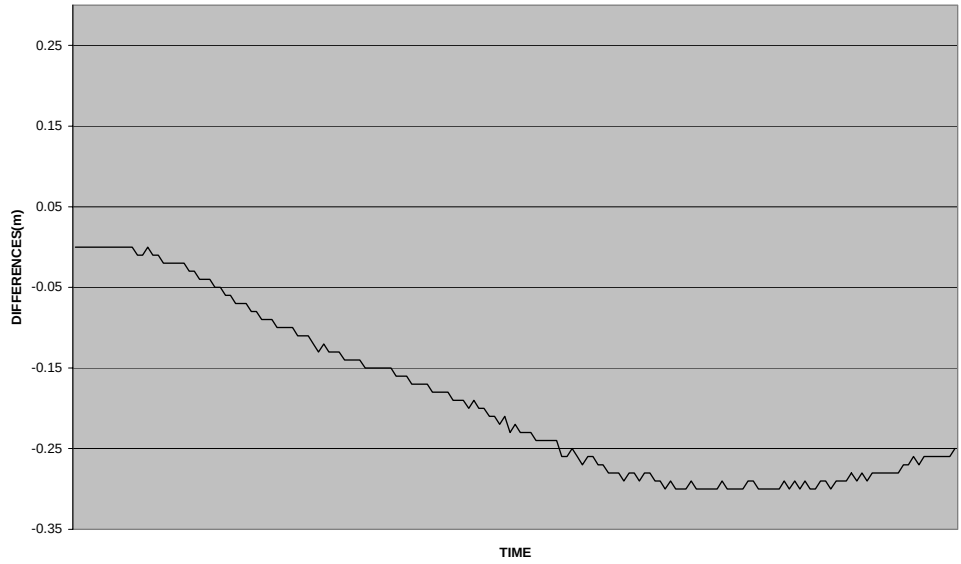

Figure 3.12. Differences of the z component of Bilsat-1 position between EGM96 and EIGEN-CG03C orbit predictions considering the degree and order of the spherical harmonic coefficients up to 50.

Figures 3.13, 3.14 and 3.15 show respectively the differences of x, y, and z components of the position of Bilsat-1 calculated for EGM96 and EIGEN-CG03C orbit prediction solutions considering the degree and order of the spherical harmonic coefficients up to the order and degree of 100.

The corresponding standard deviations for x, y, z and position of Bilsat-1 calculated for EGM96 and EIGEN-CG03C orbit prediction solutions considering the degree and order of the spherical harmonic coefficients up to 100 are calculated as 7.09 cm, 2.34 cm, 10.56 cm , and 12.93 cm respectively.

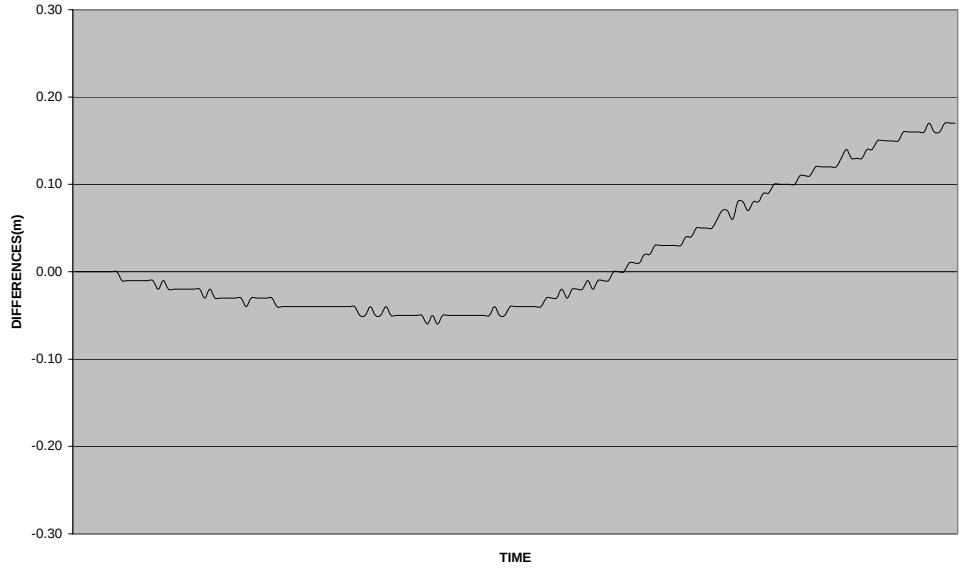

Figure 3.13. Differences of the x component of Bilsat-1 position between EGM96 and EIGEN-CG03C orbit predictions considering the degree and order of the spherical harmonic coefficients up to 100.

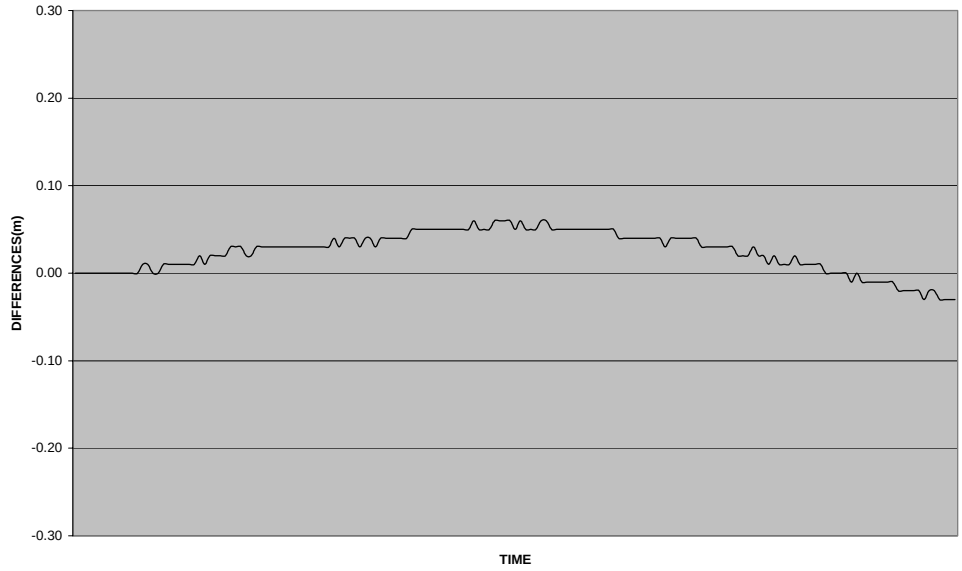

Figure 3.14. Differences of the y component of Bilsat-1 position between EGM96 and EIGEN-CG03C orbit predictions considering the degree and order of the spherical harmonic coefficients up to 100.

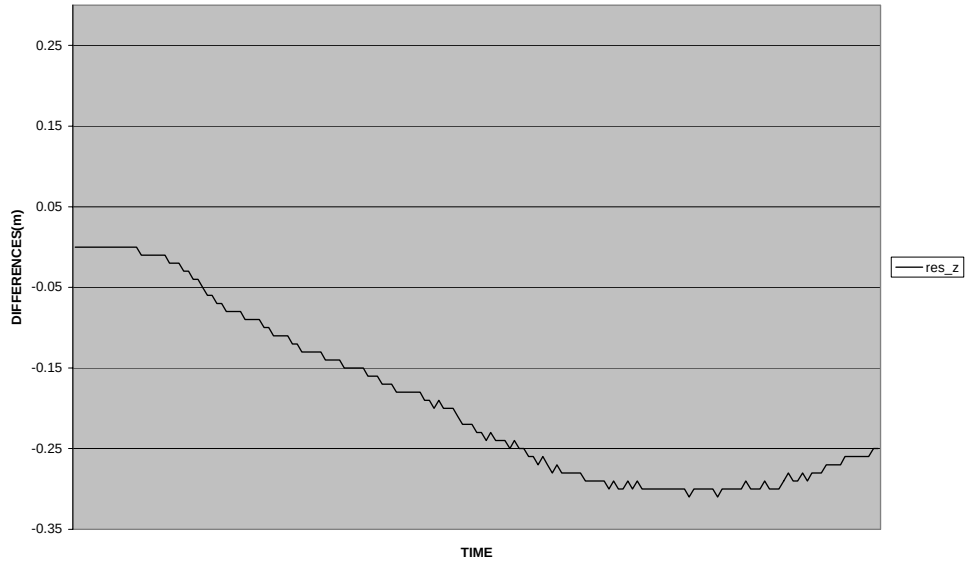

Figure 3.15. Differences of the z component of Bilsat-1 position between EGM96 and EIGEN-CG03C orbit predictions considering the degree and order of the spherical harmonic coefficients up to 100.

These results show that the effect of using two different geopotential models affect the prediction on mm level when only the J2 term is considered. The difference between the predictions of satellite positions by implying each model increase when the degree and order of the spherical harmonics coefficients increase. The rate of change decreases after the degree and order of 20 and becomes on mm level from 50 to 100 as these coefficients represent the high frequency portion of the geopotential.

Coefficients up to the degree and order of 360 are available for both models but as the rate of increase of differences become so small starting from the 50th degree and order, the comparison has not been continued after the degree and order 100 for the convenience to the objective of this study.

Table 3.1. Position error differences between EGM96 and EIGEN-CG03C geopotential models in relation with the degree and order of spherical harmonics

Degree & Order		Difference (cm)
J2	x	0.76
	y	0.49
	z	0.52
	position	0.10
10	x	4.36
	y	0.06
	z	2.71
	position	5.17
20	x	6.91
	y	2.81
	z	7.97
	position	10.91
50	x	7.09
	y	2.34
	z	10.56
	position	12.93
100	x	7.09
	y	2.34
	z	10.56
	position	12.93

3.2.1.4 Variations in Bilsat-1 Orbit Prediction Due To the Degree and Order of Spherical Harmonics

Together with comparing the effects of the geopotential model used for prediction, the effect of the degree of spherical harmonics has been investigated by calculating the differences of the orbit prediction from the solution obtained from TÜBİTAK-BİLTEN without applying any filters. Table 3.1 shows the standard deviations obtained for J2 term,

Table 3.2. Position errors in relation with the degree and order of spherical harmonics

Degree of Spherical Harmonics	Position Error (Std.Dev. -m-)
J2	352
5 x 5	215
10 x 10	31.2
20 x 20	22.5
50 x 50	24
100 x 100	23.1

Starting from the degree and order of 10, the propagation meets the expectation of tens of meters for the implementation of a reduced dynamic orbit determination algorithm using pseudorange code observables. Considering the computational burden increasing in parallel with the degree and order of spherical harmonics due to the behavior of the summing up loops of the algorithm, we can say that considering the scope and objectives of this study using the degree and order of 10, the system would benefit much more from using any higher order terms. Instead of increasing the degree and order of the coefficients, implementing a more precise numerical integration algorithm would provide better convergence prior to estimation.

3.3. KINEMATIC ORBIT DETERMINATION OF BILSAT-1

3.3.1. Observation Model

As described in Chapter 2, the performance of the kinematical orbit determination approach is directly related to the measurement model and how well the error sources are taken into account. The measurement model for the kinematical orbit determination algorithm for Bilsat-1 has been established based on code pseudorange measurements of L1 frequency. Let us remember the pseudorange measurement model in equation 2.33 which is,

$$PR_i = \rho + c.\delta t_u = c.\tau_i = ((X_i - X_B)^2 + (Y_i - Y_B)^2 + (Z_i - Z_B)^2)^{1/2} + c.\delta t_u \qquad (3.5)$$

In equation 3.5, the pseudorange measurements are dependent on the receiver coordinates in a non-linear fashion. Although closed form solutions are available, the typical solution is based on the linearization of the measurement equations. This approach is straightforward and converges quickly, and allows linear analysis techniques to be applied. (Farrel and Barth, 1998)

Linearizing the equation 3.5 for four observations at one epoch and estimating the parameters with Gauss Markoff model;

$$\mathbf{X\beta} = \mathbf{y} + \mathbf{e} \qquad (3.6)$$

$$\begin{bmatrix} \rho^1(x) \\ \rho^2(x) \\ \rho^3(x) \\ \rho^4(x) \end{bmatrix} + \begin{bmatrix} e_1 \\ e_2 \\ e_3 \\ e_4 \end{bmatrix} = \begin{bmatrix} \rho^1(x_0) \\ \rho^2(x_0) \\ \rho^3(x_0) \\ \rho^4(x_0) \end{bmatrix} + \mathbf{X} \begin{bmatrix} (x - x_0) \\ (y - y_0) \\ (z - z_0) \\ (c\delta_t - c\delta_{t_0}) \end{bmatrix} \qquad (3.7)$$

where

$$\mathbf{X} = \begin{bmatrix} \frac{\delta\rho^1}{\delta_x} & \frac{\delta\rho^1}{\delta_y} & \frac{\delta\rho^1}{\delta_z} & 1 \\ \frac{\delta\rho^2}{\delta_x} & \frac{\delta\rho^2}{\delta_y} & \frac{\delta\rho^2}{\delta_z} & 1 \\ \frac{\delta\rho^3}{\delta_x} & \frac{\delta\rho^3}{\delta_y} & \frac{\delta\rho^3}{\delta_z} & 1 \\ \frac{\delta\rho^4}{\delta_x} & \frac{\delta\rho^4}{\delta_y} & \frac{\delta\rho^4}{\delta_z} & 1 \end{bmatrix} \tag{3.8}$$

One gets the estimated receiver positions by;

$$\hat{\boldsymbol{\beta}} = (\boldsymbol{X}^T \boldsymbol{X})^{-1} \boldsymbol{X}^T \boldsymbol{y} \tag{3.9}$$

and the covariance matrix by;

$$D(\hat{\boldsymbol{\beta}}) = \sigma^2 (\boldsymbol{X}^T \boldsymbol{X})^{-1} \tag{3.10}$$

Algorithms based on single frequency pseudorange measurements are weaker in nature than measurements as the opportunities of eliminating errors are limited. In case of dealing with single frequency pseudorange measurements it is not possible to take into account the atmospheric corrections without modeling them properly and it is a tedious task to accomplish. The most appropriate and practical way to utilize the single frequency measurements for better precision leaves us with estimating the receiver clock error by equations 3.6 to 3.10 including one additional measurement for the solution and modeling the satellite clock error in order to compensate the two main error sources. In addition, the more precise ephemerides lead to a more precise solution.

3.3.2 Rapid, Ultra Rapid and Final IGS GPS Ephemerides Products

The International GNSS Service (IGS), formerly the International GPS Service, is a voluntary federation of more than 200 worldwide agencies that pool resources and

permanent GPS & GLONASS station data to generate precise GPS & GLONASS products. The IGS global system of satellite tracking stations, Data Centers, and Analysis Centers puts high-quality GPS data and data products on line in near real time to meet the objectives of a wide range of scientific and engineering applications and studies. The IGS collects, archives, and distributes GPS observation data sets of sufficient accuracy to satisfy the objectives of a wide range of applications and experimentation. These data sets are used by the IGS to generate the data products mentioned above which are made available to interested users through the Internet. (IGS, 2005)

Table 3.3. IGS products, accuracy and availability

GPS Satellite Ephemerides /Satellite & Station Clocks		**Accuracy**	**Latency**	**Updates**	**Sample Interval**
Broadcast	orbits	~160 cm	real time	--	daily
	Sat. clocks	~7 ns			
Ultra-Rapid (predicted half)	orbits	~10 cm	real time	four times daily	15 min
	Sat. clocks	~5 ns			
Ultra-Rapid (observed half)	orbits	<5 cm	3 hours	four times daily	15 min
	Sat. clocks	~0.2 ns			
Rapid	orbits	<5 cm	17 hours	daily	15 min
	Sat. & Stn. clocks	0.1 ns			5 min
Final	orbits	<5 cm	~13 days	weekly	15 min
	Sat. & Stn. clocks	<0.1 ns			5 min

3.3.2.1 Interpolation of Precise Ephemerides and Satellite Clock Corrections

When processing GPS measurements at epochs that do not coincide with grid points of the IGS ephemeris products, the position and clock offset of the observed GPS satellite have to be obtained by interpolation. (Montenbruck et al., 2005)

An 8th order Lagrange polynomial interpolation has been applied to the ephemerides data obtained from IGS in order to find the positions of the GPS satellites at the time of observation.

3.3.3 Parameter Estimation on the Basis of Rapid, Ultra Rapid and Final IGS GPS Ephemerides Products

In order to test the effects of GPS satellite ephemerides and satellite clock accuracies on kinematic orbit determination, Ultra Rapid, Rapid and Final GPS ephemerides and satellite clock products of IGS have been downloaded from its web site. Kinematic orbit determination has been performed by using final, rapid and ultra rapid ephemerides and satellite clock corrections.

Figures 3.15, 3.16, 3.17, 3.18, 3.19, 3.20 show the residuals of position (x, y, z) and velocities (vx, vy, vz) of kinematic orbit determination solution from the solution obtained from TÜBİTAK-BİLTEN by using ultra rapid GPS ephemerides and satellite clock products of IGS.

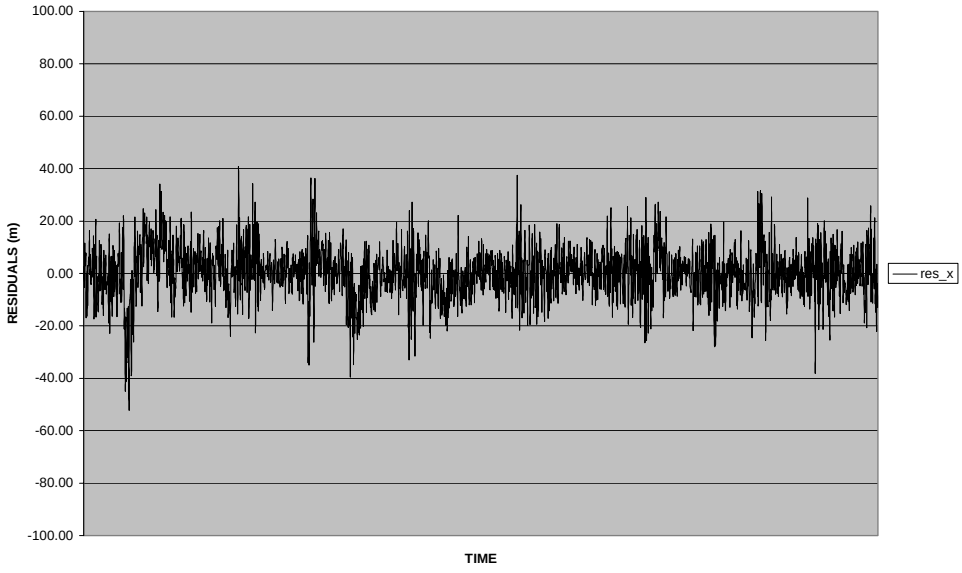

Figure 3.16. Residuals of kinematic orbit determination (x component of position) with IGS ultra rapid ephemerides from TÜBİTAK-BİLTEN solution.

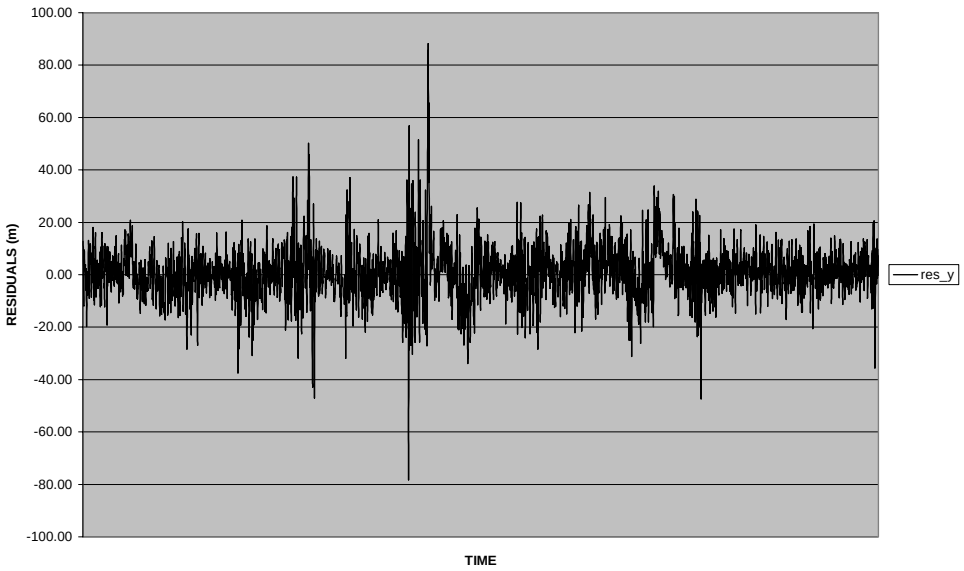

Figure 3.17. Residuals of kinematic orbit determination (y component of position) with IGS ultra rapid ephemerides from TÜBİTAK-BİLTEN solution.

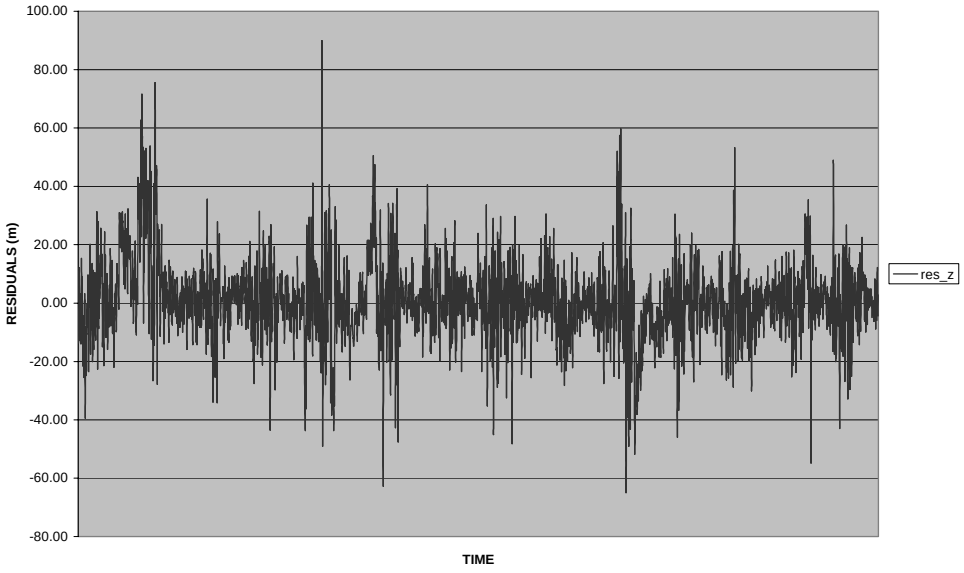

Figure 3.18. Residuals of kinematic orbit determination (z component of position) with IGS ultra rapid ephemerides from TÜBİTAK-BİLTEN solution.

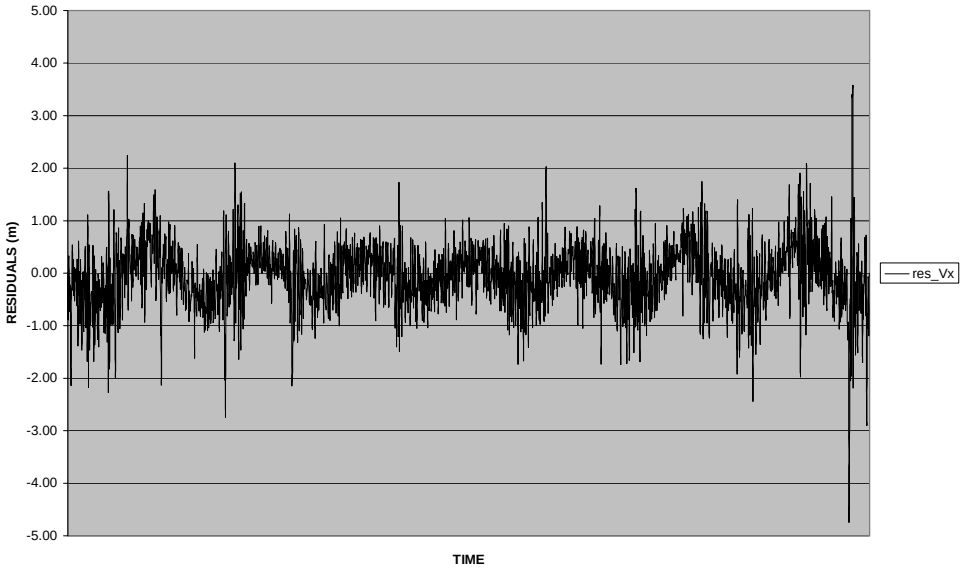

Figure 3.19. Residuals of kinematic orbit determination (x component of velocity) with IGS ultra rapid ephemerides from TÜBİTAK-BİLTEN solution.

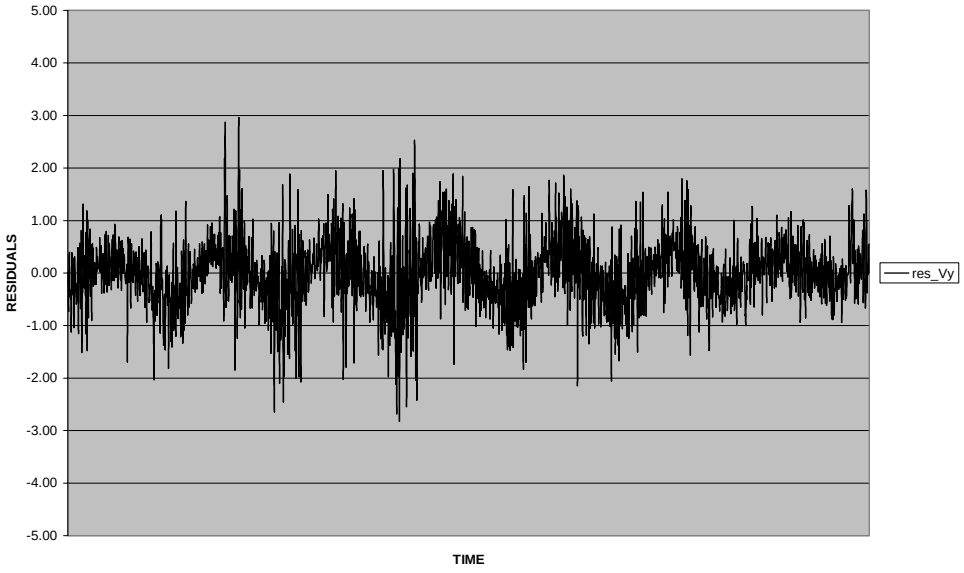

Figure 3.20. Residuals of kinematic orbit determination (y component of velocity) with IGS ultra rapid ephemerides from TÜBİTAK-BİLTEN solution.

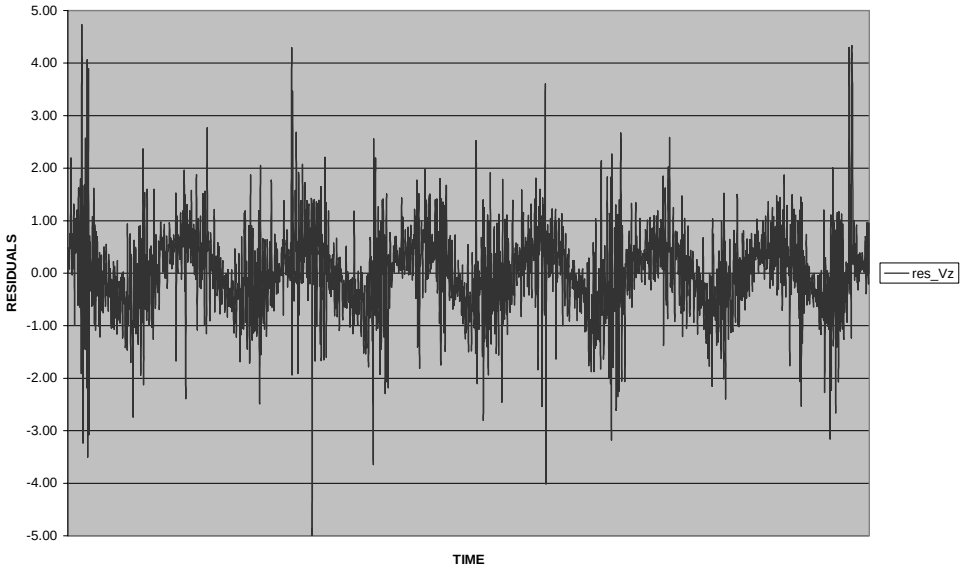

Figure 3.21. Residuals of kinematic orbit determination (z component of velocity) with IGS ultra rapid ephemerides from TÜBİTAK-BİLTEN solution.

Figures 3.21, 3.22, 3.23, 3.24, 3.25, 3.26 show the residuals of position (x, y, z) and velocities (vx, vy, vz) of kinematic orbit determination solution from the solution obtained from TÜBİTAK-BİLTEN by using rapid GPS ephemerides and satellite clock products of IGS.

Figures 3.27, 3.28, 3.29, 3.30, 3.31, 3.32 show the residuals of position (x, y, z) and velocities (vx, vy, vz) of kinematic orbit determination solution from the solution obtained from TÜBİTAK-BİLTEN by using final GPS ephemerides and satellite clock products of IGS.

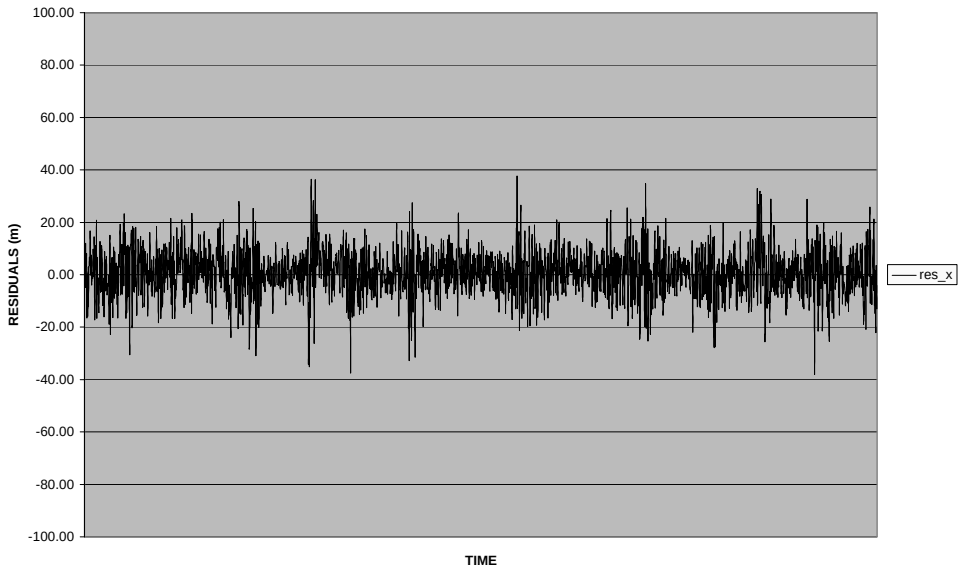

Figure 3.22. Residuals of kinematic orbit determination (x component of position) with IGS rapid ephemerides from TÜBİTAK-BİLTEN solution.

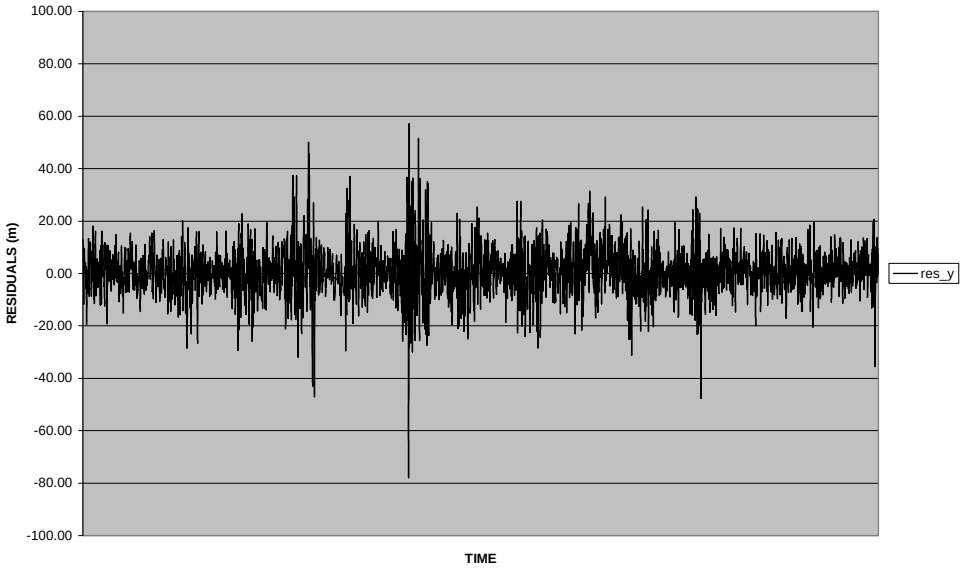

Figure 3.23. Residuals of kinematic orbit determination (y component of position) with IGS rapid ephemerides from TÜBİTAK-BİLTEN solution.

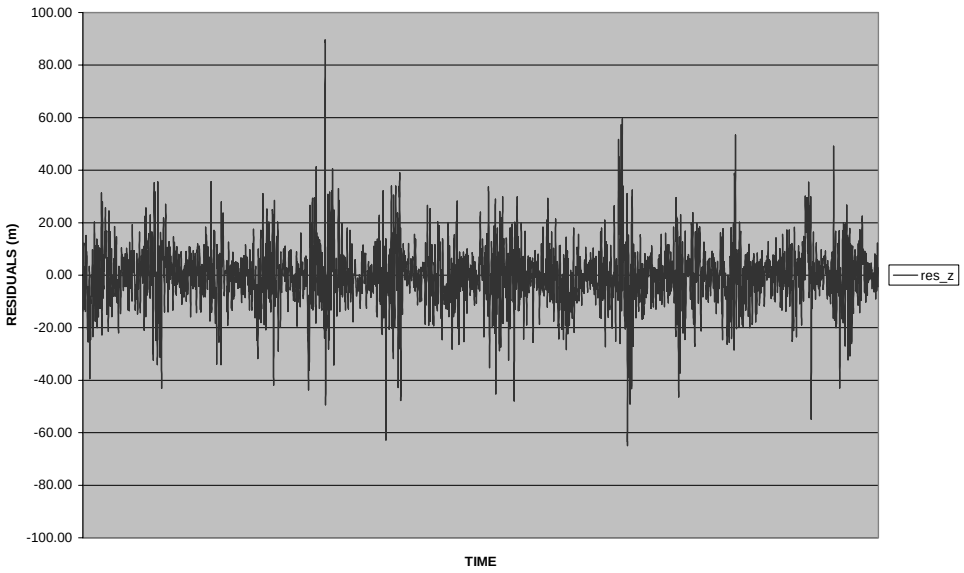

Figure 3.24. Residuals of kinematic orbit determination (z component of position) with IGS rapid ephemerides from TÜBİTAK-BİLTEN solution.

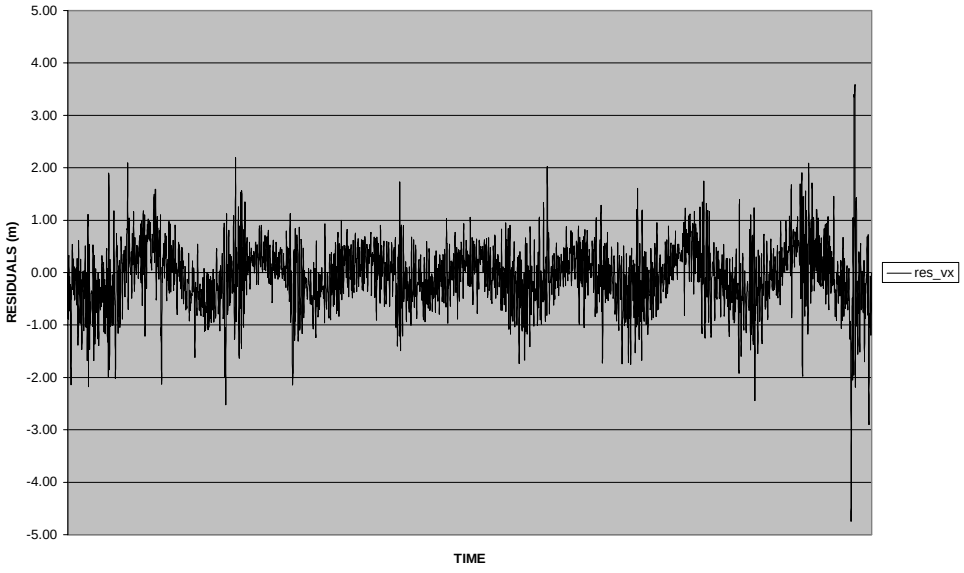

Figure 3.25. Residuals of kinematic orbit determination (x component of velocity) with IGS rapid ephemerides from TÜBİTAK-BİLTEN solution.

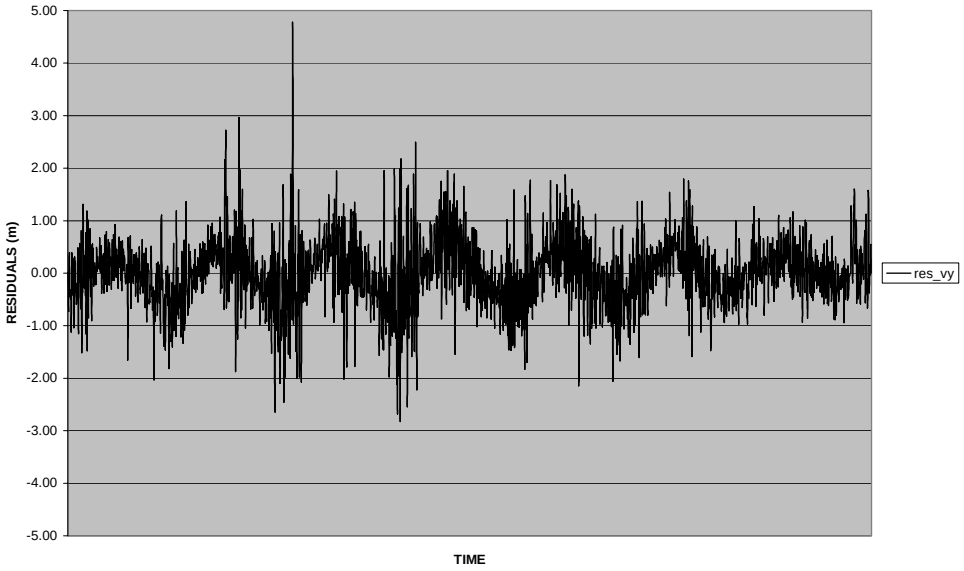

Figure 3.26. Residuals of kinematic orbit determination (y component of velocity) with IGS rapid ephemerides from TÜBİTAK-BİLTEN solution.

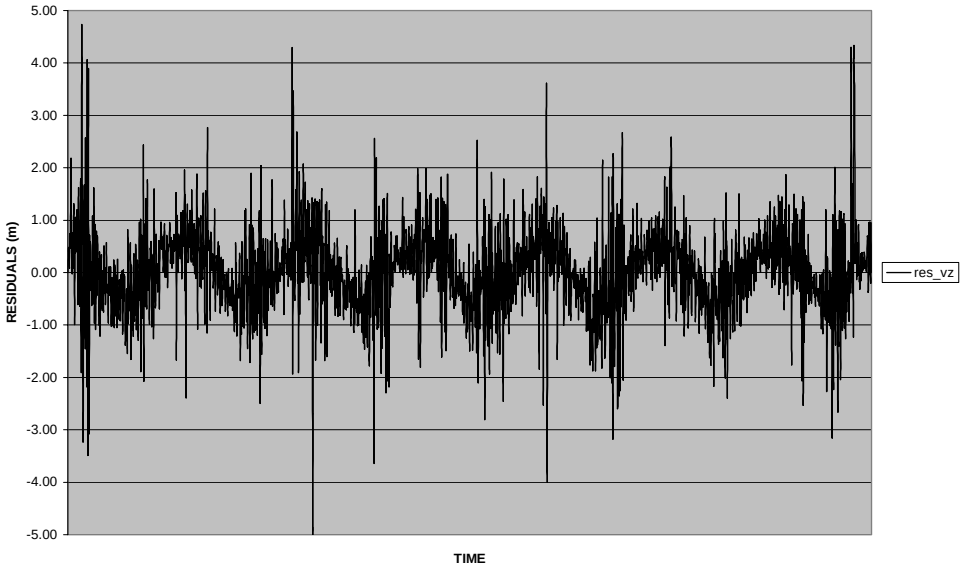

Figure 3.27. Residuals of kinematic orbit determination (z component of velocity) with IGS rapid ephemerides from TÜBİTAK-BİLTEN solution.

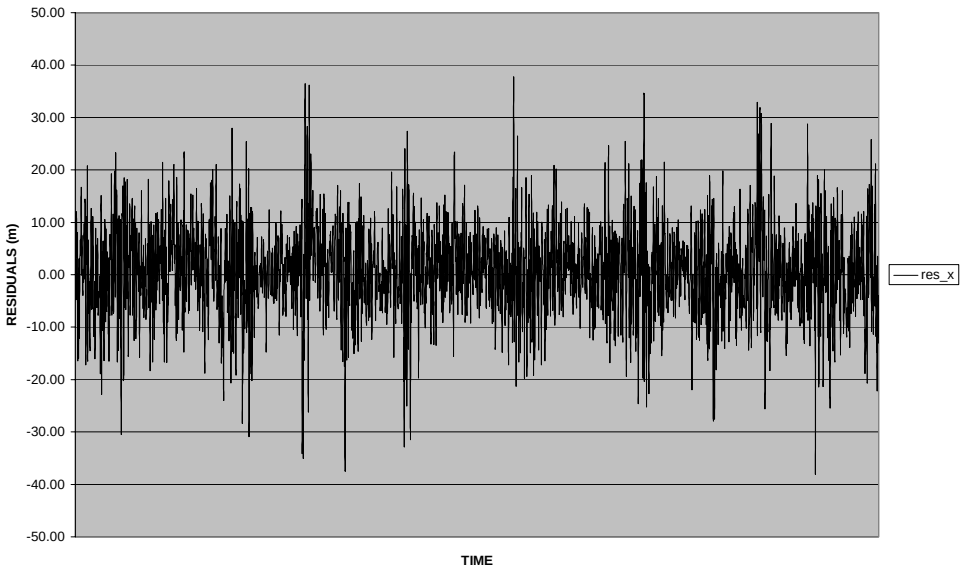

Figure 3.28. Residuals of kinematic orbit determination (x component of position) with IGS final ephemerides from TÜBİTAK-BİLTEN solution.

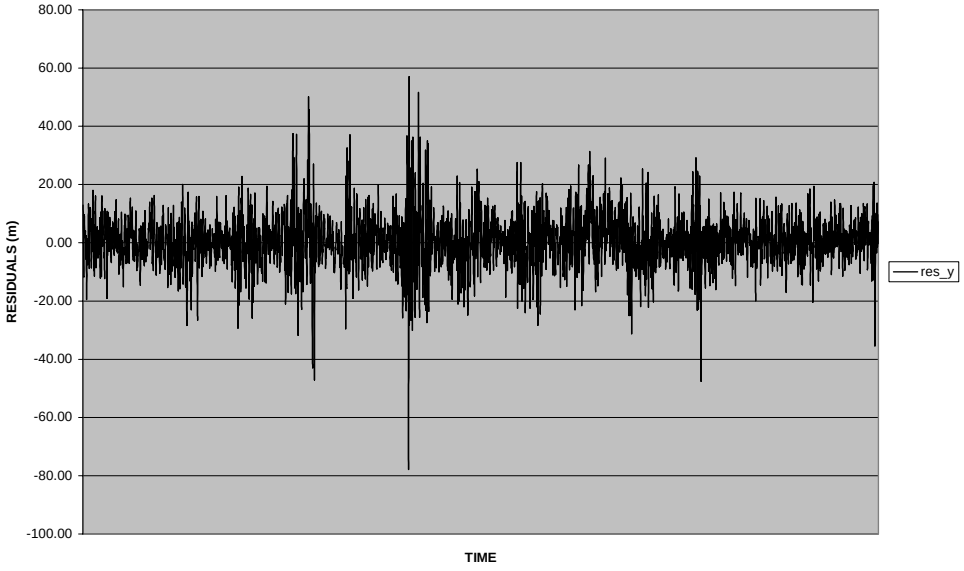

Figure 3.29. Residuals of kinematic orbit determination (y component of position) with IGS final ephemerides from TÜBİTAK-BİLTEN solution.

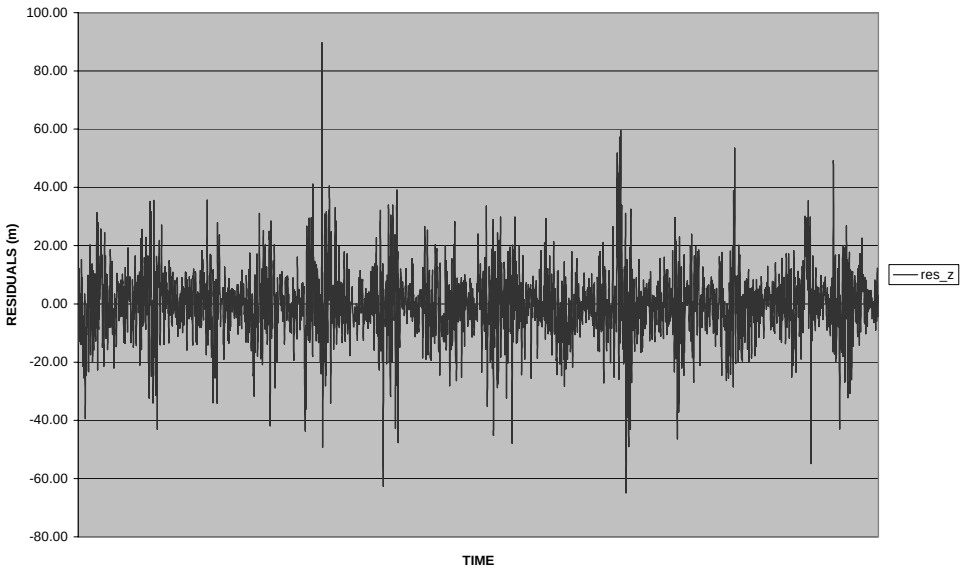

Figure 3.30. Residuals of kinematic orbit determination (z component of position) with IGS final ephemerides from TÜBİTAK-BİLTEN solution.

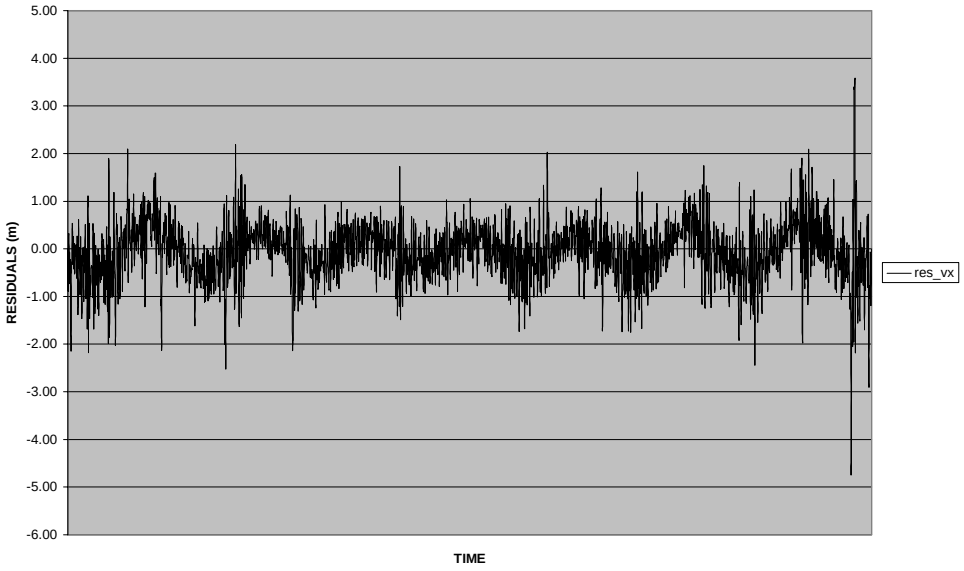

Figure 3.31. Residuals of kinematic orbit determination (x component of velocity) with IGS final ephemerides from TÜBİTAK-BİLTEN solution.

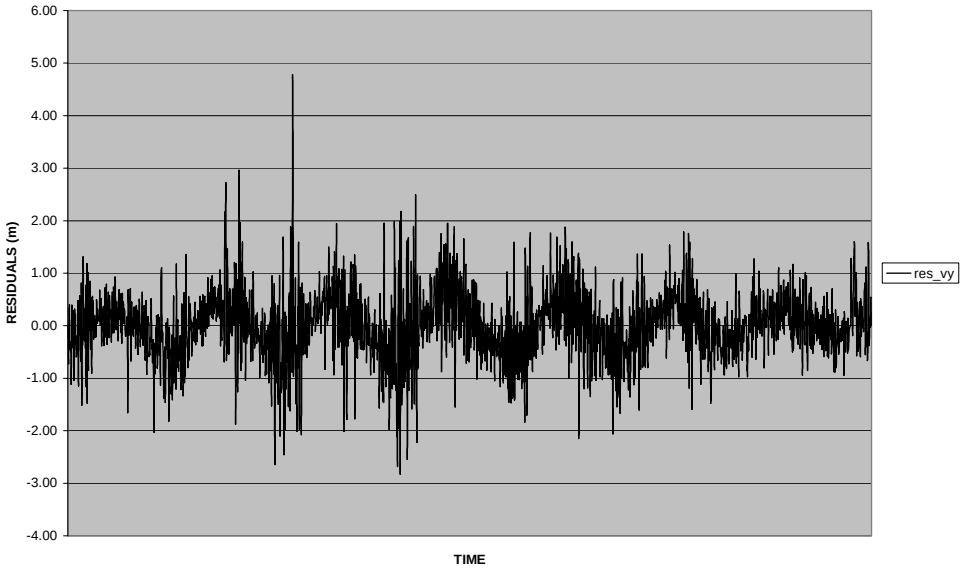

Figure 3.32. Residuals of kinematic orbit determination (y component of velocity) with IGS final ephemerides from TÜBİTAK-BİLTEN solution.

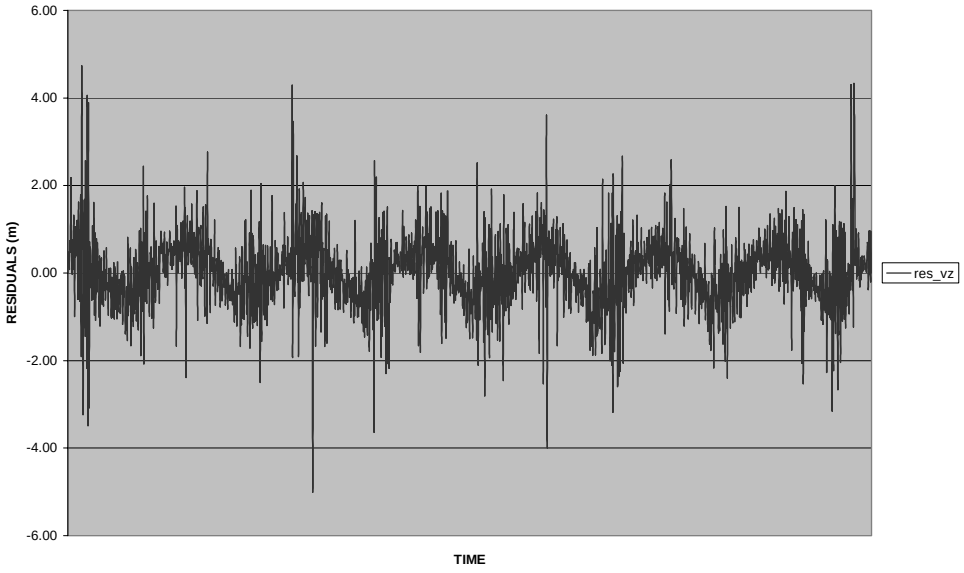

Figure 3.33. Residuals of kinematic orbit determination (z component of velocity) with IGS final ephemerides from TÜBİTAK-BİLTEN solution.

Table 3.4 shows the errors of the kinematic orbit determination with ultra rapid, rapid, and final IGS ephemerides and satellite clock products from the solution obtained from TÜBİTAK-BİLTEN as standard deviations.

Table 3.4. Kinematic OD position and velocity errors (IGS products comparison)

Orbit Determination	**Standard Deviation (m)**							
	x	**y**	**z**	**pos**	**vx**	**vy**	**vz**	**vel**
Kinematic OD (Final Ephemerides)	8.76	9.58	11.86	17.58	0.62	0.97	0.95	1.49
Kinematic OD (Rapid Ephemerides)	8.76	9.58	11.86	17.58	0.62	0.97	0.95	1.49
Kinematic OD (Ultra Rapid Ephemerides)	9.74	10.42	13.81	19.85	0.62	0.97	0.95	1.49

It is observed from the results that using IGS final ephemerides products instead of rapid products for kinematic orbit determination with single frequency pseudorange observables does not improve the accuracy but there's improvement in positional accuracy when using rapid or final ephemerides instead of ultra rapid ephemerides. It is also observed that the improvement in position does not affect overall error of velocities.

3.4. REDUCED DYNAMIC ORBIT DETERMINATION OF BILSAT-1

3.4.1. Influence of State Transition Matrices

State transition is one of the key issues in reduced dynamic orbit determination. Kalman filtering scheme utilizes the state transition matrix for the time update of the state. In other words, for the prediction of the state in the next time step using the current estimated state.

The function of the transition matrix is to relate the rectangular coordinate variations between the times t_k and t_{k+1}. Also, it can be used to relate the residuals between the

observed and calculated measurements in the orbit determination. The more precise the transition matrix, the better the orbit determination is. (Chiaradia et al, 2000)

State transition matrix is normaly integrated together with the integration of the equations of motion.

$$\dot{\mathbf{\Phi}} = \mathbf{F}\mathbf{\Phi} \tag{3.11}$$

Another suggested method consists of propagating the state vector using complete force model and, then, to compute the transition matrix using a simplified force model. The proposed method is used in this work and the transition matrix is propagated by the Markley's method at the same time. (Chiaradia et al., 1999)

The Markley's method uses two states, one in t_{k-1} time and other in t_k time, and calculates the transition matrix between them using m, J2, D_t, the radius of the Earth, and the two states. In this case, the effect of Earth flattening is the most influent factor in the process.

The state transition's differential equation is defined as

$$\frac{d\mathbf{\Phi}(t,t_0)}{dt} = \begin{bmatrix} \mathbf{0} & \mathbf{I} \\ \mathbf{G}(t) & \mathbf{0} \end{bmatrix} \mathbf{\Phi}(t,t_0) \tag{3.12}$$

where $\mathbf{\Phi}(t,t_0) \equiv \mathbf{I}$ is the initial condition,

$$\mathbf{\Phi}(t,t_0) = \begin{bmatrix} \dfrac{d\mathbf{r}}{d\mathbf{r}_0} & \dfrac{d\mathbf{r}}{d\mathbf{v}_0} \\ \dfrac{d\mathbf{v}}{d\mathbf{r}_0} & \dfrac{d\mathbf{v}}{d\mathbf{v}_0} \end{bmatrix} \mathbf{\Phi}(t,t_0) \tag{3.13}$$

where

r, v	cartesian state at the instant t
$\mathbf{r_0}$, $\mathbf{v_0}$	cartesian state at t_0
0	matrix 3 x 3 of zeros
$\mathbf{G}(t) \equiv \frac{d\mathbf{f}(\mathbf{r},t)}{d\mathbf{r}}$	gradient matrix
f(**r**,t)	accelerations on the satellite

Developing the Markley's method, the transition matrix for position and velocity is given by

$$\mathbf{\Phi}(t,t_0) \approx \begin{bmatrix} \mathbf{\Phi}_{rr} & \mathbf{\Phi}_{rv} \\ \mathbf{\Phi}_{vr} & \mathbf{\Phi}_{vv} \end{bmatrix}_{6\times 6} \tag{3.14}$$

where

$$\begin{aligned} \mathbf{\Phi}_{rr} &\equiv \mathbf{I} + (2\mathbf{G}_0 + \mathbf{G})\frac{(\Delta t)^2}{6} \\ \mathbf{\Phi}_{rv} &\equiv \mathbf{I}\Delta t + (\mathbf{G}_0 + \mathbf{G})\frac{(\Delta t)^3}{12} \\ \mathbf{\Phi}_{vr} &\equiv (\mathbf{G}_0 + \mathbf{G})\frac{(\Delta t)}{2} \\ \mathbf{\Phi}_{vv} &\equiv \mathbf{I} + (\mathbf{G}_0 + 2\mathbf{G})\frac{(\Delta t)^2}{6} \end{aligned} \tag{3.15}$$

where

$\Delta t \equiv t_k - t_0$ and $\mathbf{G}(0) \equiv \mathbf{G}(t_0)$

The **G** and therefore $\mathbf{\Phi}_{rr}, \mathbf{\Phi}_{rv}, \mathbf{\Phi}_{vr}, \mathbf{\Phi}_{vv}$ are symmetric if the perturbation is derived from potential. The **G** gradient matrix, including only the central force and the J_2, is given by

$$\mathbf{G}(t) = \frac{d\mathbf{f}(\mathbf{r},t)}{d\mathbf{r}} = \begin{bmatrix} \frac{df_x}{dx} & \frac{df_x}{dy} & \frac{df_x}{dz} \\ \frac{df_y}{dx} & \frac{df_y}{dy} & \frac{df_y}{dz} \\ \frac{df_z}{dx} & \frac{df_z}{dy} & \frac{df_z}{dz} \end{bmatrix} \tag{3.16}$$

The accelerations due to Earth's flattening are given by

$$\begin{aligned} f_x &= \frac{-\mu x}{r^3}\left[1+\frac{3}{2}\frac{j_2 R_e^2}{r^2}\left(1-\frac{5z^2}{r^2}\right)\right] \\ f_y &= \frac{y}{x} f_x \\ f_z &= \frac{-\mu z}{r^3}\left[1+\frac{3}{2}\frac{j_2 R_e^2}{r^2}\left(3-\frac{5z^2}{r^2}\right)\right] \end{aligned} \tag{3.17}$$

State transition matrix computation has been performed both by the integration of the equations of motion and alternatively with Markley's method. Figures 3.33, 3.34, 3.35, 3.36, 3.37 and 3.38 show the residuals of position (x, y, z) and velocities (vx, vy, vz) of the reduced dynamic orbit determination solution from the solution obtained from TÜBİTAK-BİLTEN using state transition matrix calculated by integration of equations of motion.

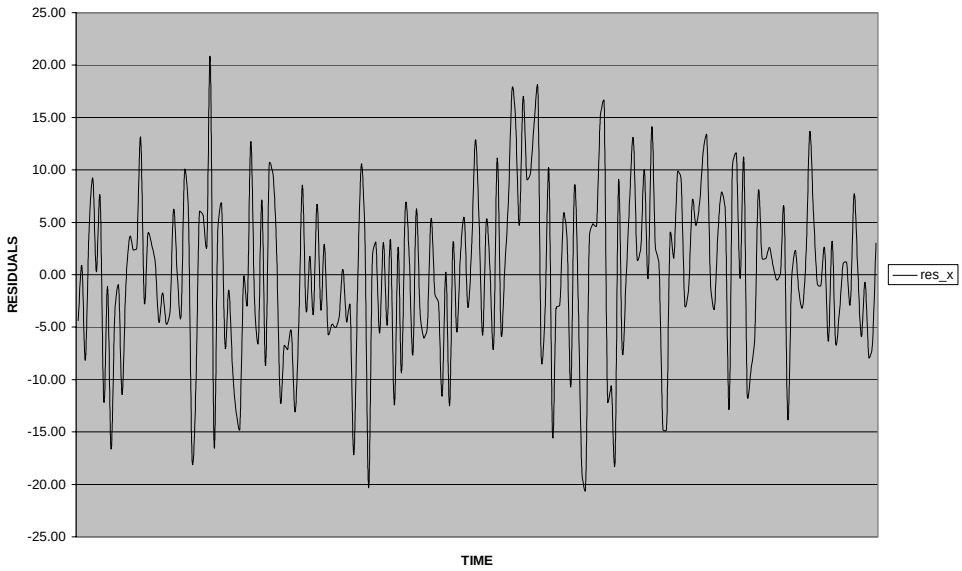

Figure 3.34. Residuals of reduced dynamic orbit determination (x) with integrated state transition from TÜBİTAK-BİLTEN solution.

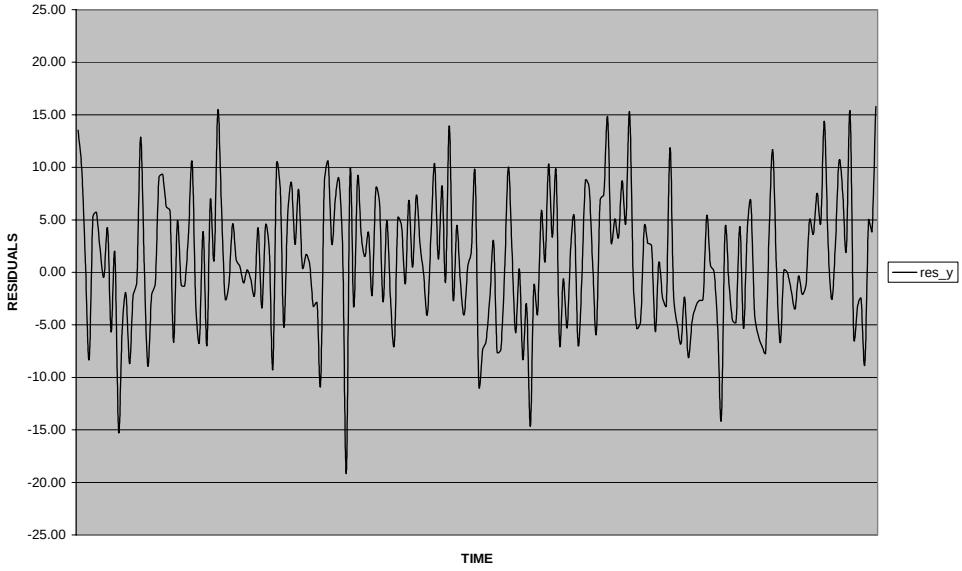

Figure 3.35. Residuals of reduced dynamic orbit determination (y) with integrated state transition from TÜBİTAK-BİLTEN solution.

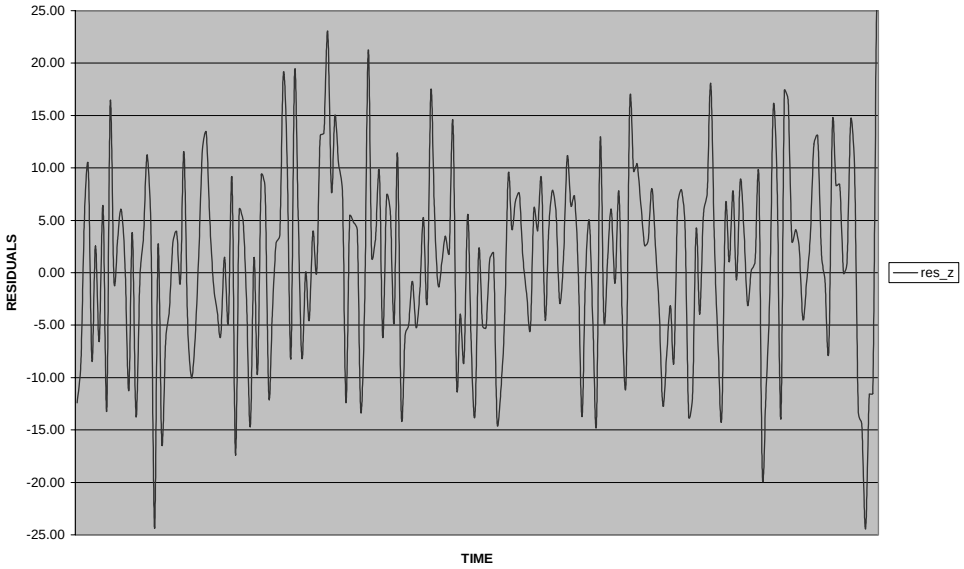

Figure 3.36 Residuals of reduced dynamic orbit determination (z) with integrated state transition from TÜBİTAK-BİLTEN solution.

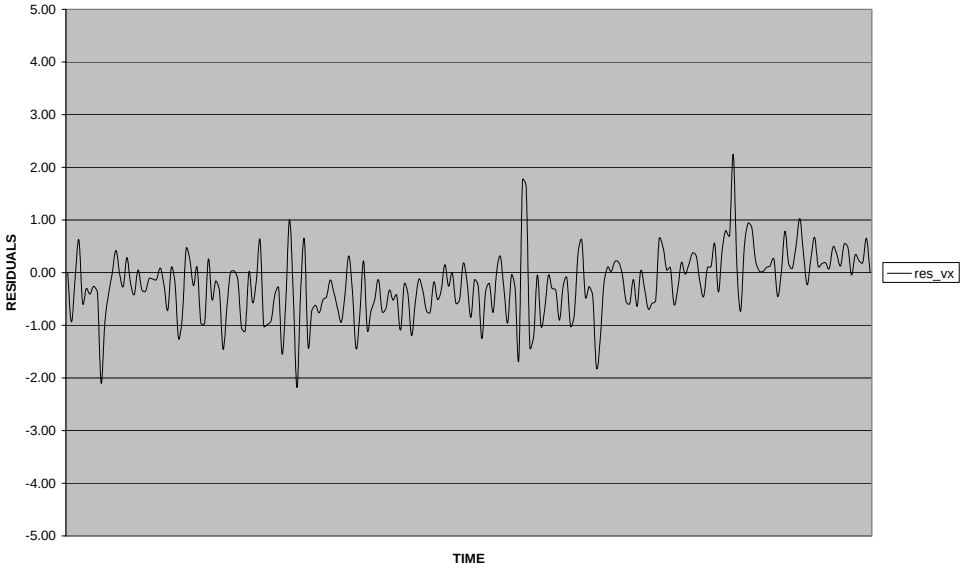

Figure 3.37. Residuals of reduced dynamic orbit determination (vx) with integrated state transition from TÜBİTAK-BİLTEN solution.

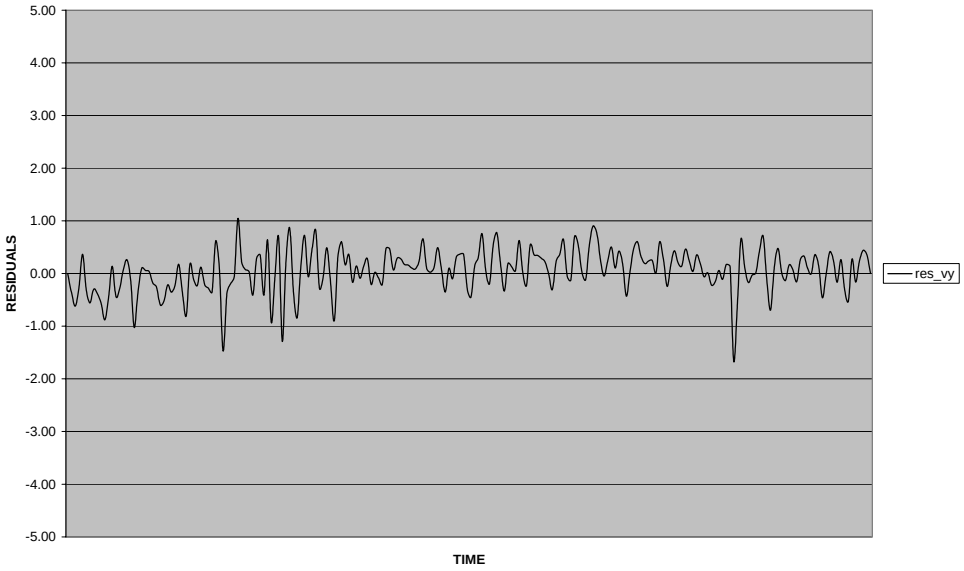

Figure 3.38. Residuals of reduced dynamic orbit determination (vy) with integrated state transition from TÜBİTAK-BİLTEN solution.

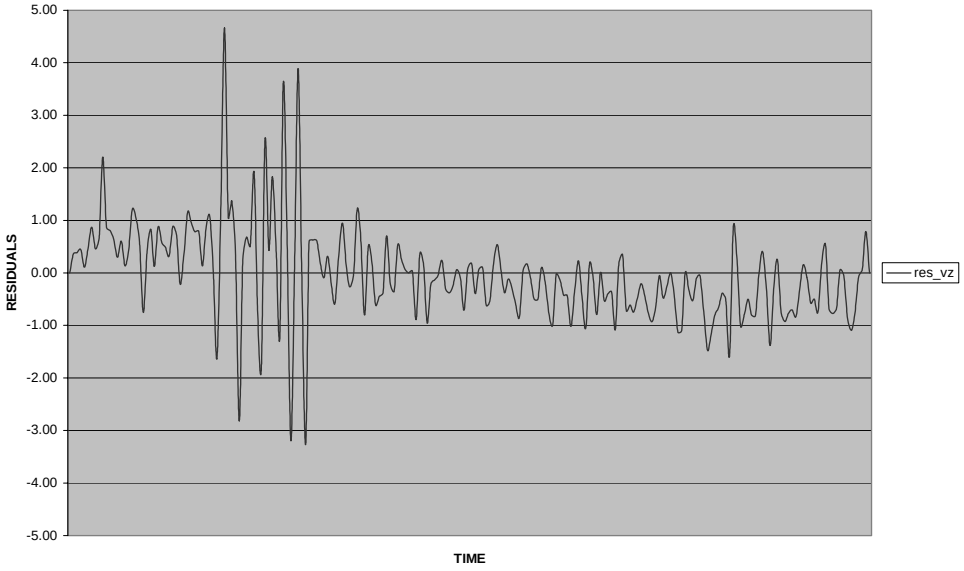

Figure 3.39 Residuals of reduced dynamic orbit determination (vz) with integrated state transition from TÜBİTAK-BİLTEN solution.

Figures 3.39, 3.40, 3.41, 3.42, 3.43 and 3.44 show the residuals of position (x, y, z) and velocities (vx, vy, vz) of the reduced dynamic orbit determination solution from the solution obtained from TÜBİTAK-BİLTEN using Markley's state transition matrix

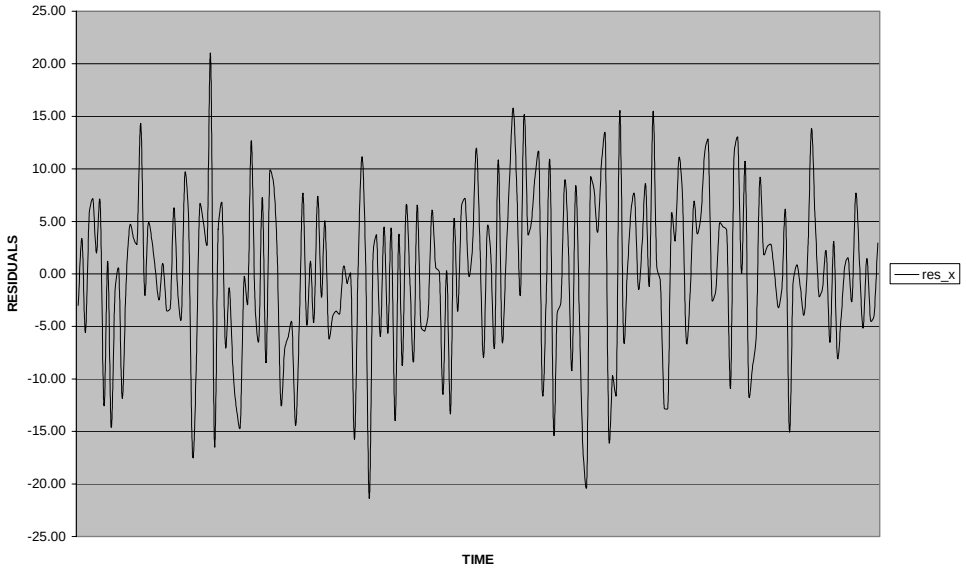

Figure 3.40. Residuals of reduced dynamic orbit determination (x) with Markley's state transition from TÜBİTAK-BİLTEN solution.

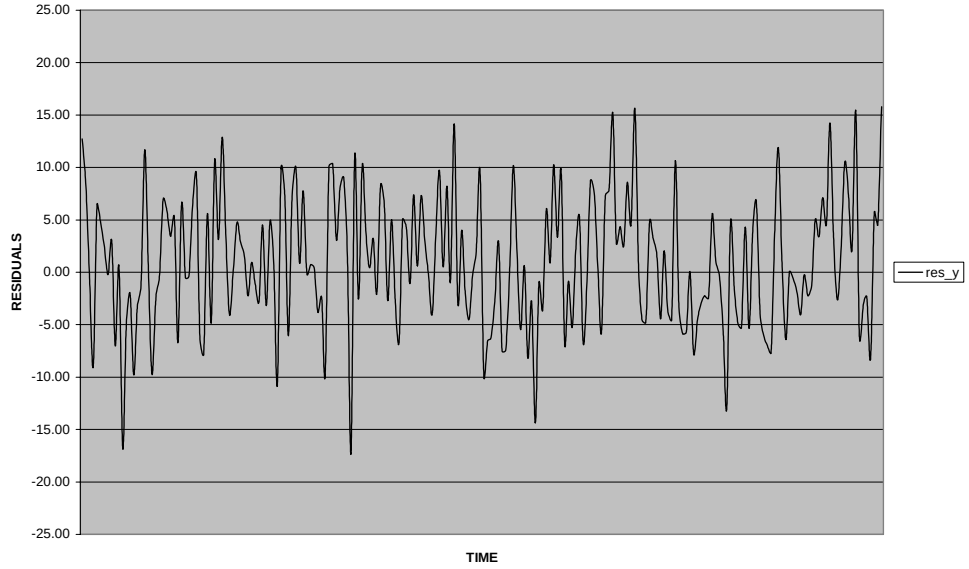

Figure 3.41. Residuals of reduced dynamic orbit determination (y) with Markley's state transition from TÜBİTAK-BİLTEN solution.

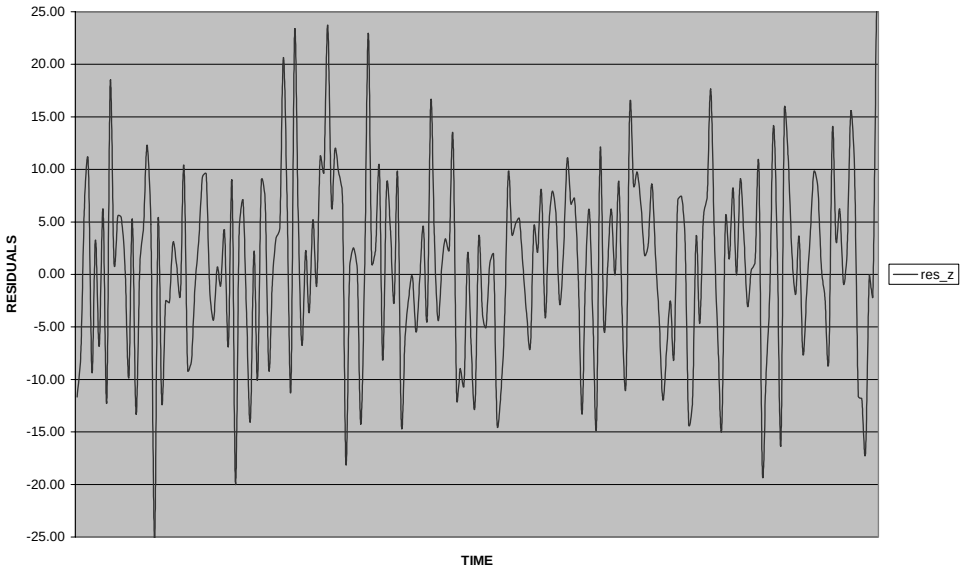

Figure 3.42. Residuals of reduced dynamic orbit determination (z) with Markley's state transition from TÜBİTAK-BİLTEN solution.

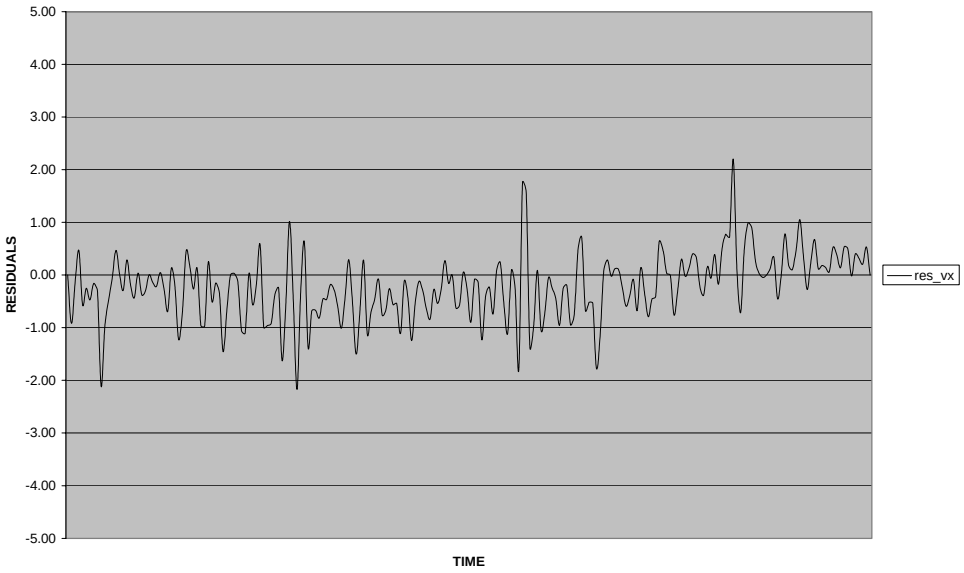

Figure 3.43. Residuals of reduced dynamic orbit determination (vx) with Markley's state transition from TÜBİTAK-BİLTEN solution.

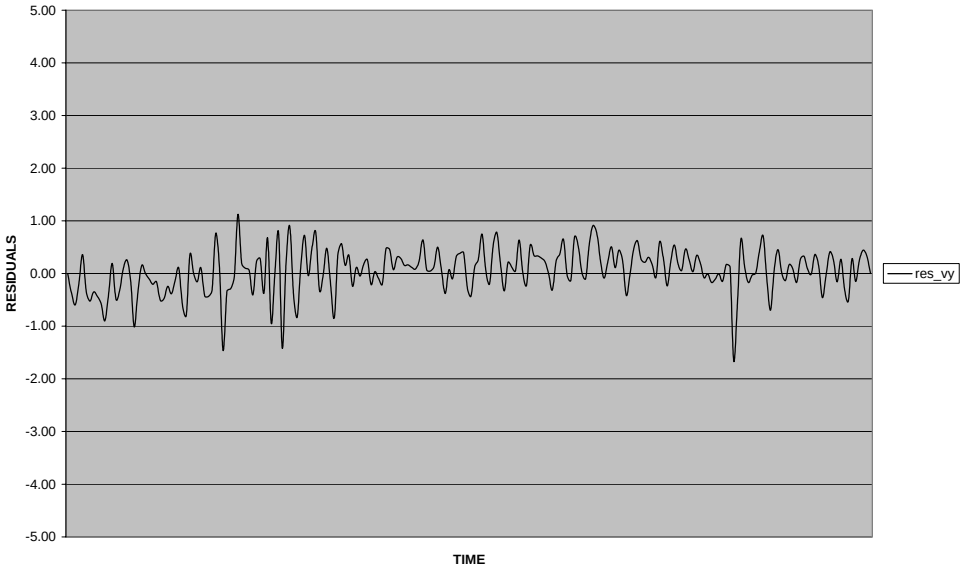

Figure 3.44. Residuals of reduced dynamic orbit determination (vy) with Markley's state transition from TÜBİTAK-BİLTEN solution.

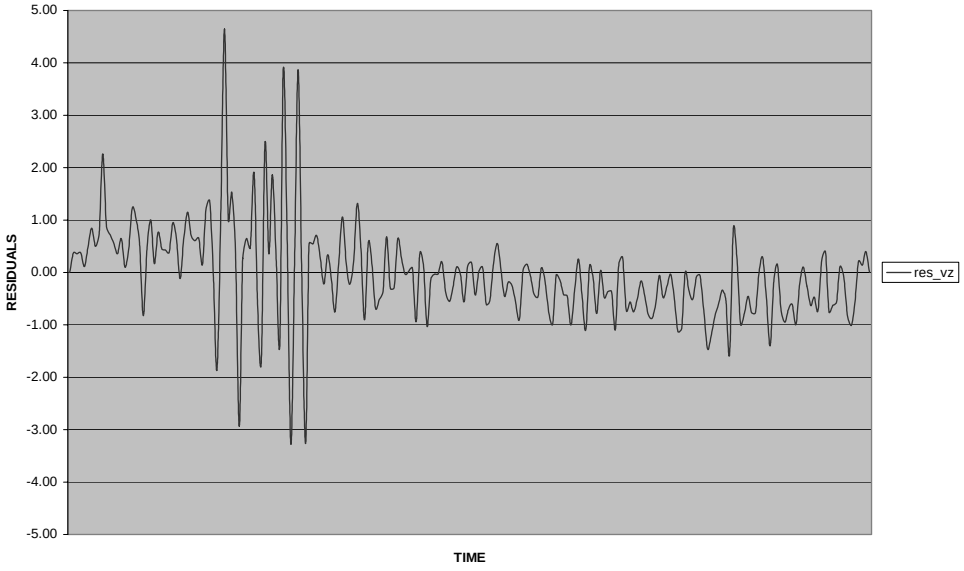

Figure 3.45. Residuals of reduced dynamic orbit determination (vz) with Markley's state transition from TÜBİTAK-BİLTEN solution.

Table 3.5 shows the errors of the reduced dynamic orbit determination with integrated state transition and Markley's state transition from the solution obtained from TÜBİTAK-BİLTEN as standard deviations.

Table 3.5. Reduced Dynamic OD position and velocity errors (transition Matrix Comparison)

Orbit Determination	**Standard Deviation (m)**							
	x	**y**	**z**	**pos**	**vx**	**vy**	**vz**	**vel**
Reduced Dynamic OD Markley's Transition -1 Hour-	7.80	6.32	8.78	13.34	0.53	0.46	1.09	1.29
Reduced Dynamic OD Integrated Transition -1 Hour-	8.13	6.32	9.11	13.74	0.52	0.45	1.06	1.27

As seen in Table 3.5 the results obtained from both methods are so close to each other. Integrating the equations of motion is a much more time consuming process than the explicit calculation of Markley's state transition matrix. Using Markley's method instead of integrating the state transition matrix results in saving computational time within the same accuracy expectation.

3.4.2. Numerical Integration

Runge-Kutta 4^{th} order numerical integration has been used for the integration of equations of motion and the state for Bilsat-1 reduced dynamic orbit determination. Step size of the numerical integration is of importance as it is also another time saving issue. The pseudorange data of Bilsat-1 has an interval of 15 seconds in general. Effect of different step sizes have been investigated in order to find out if there's considerable change in the accuracy if the integration is held either with 1 second, 5 seconds, 10 seconds or 15 seconds of step size which is the general interval of Bilsat-1 data obtained from TÜBİTAK-BİLTEN.

Table 3.6 shows the errors of the reduced dynamic orbit determination with 1, 5, 10 or 15 seconds of step sizes applied during numerical integration from the solution obtained from TÜBİTAK-BİLTEN as standard deviations.

Table 3.6. Reduced Dynamic OD position and velocity errors (Numerical Integration Step Size Comparison)

Orbit Determination	**Standard Deviation (m)**							
	x	**y**	**z**	**pos**	**vx**	**vy**	**vz**	**vel**
Reduced Dynamic OD 1 sec Integration Step -1 Hour-	8.13	6.32	9.11	13.74	0.52	0.45	1.06	1.27
Reduced Dynamic OD 5 sec Integration Step -1 Hour-	8.13	6.32	9.11	13.74	0.52	0.45	1.06	1.27
Reduced Dynamic OD 10 sec Integration Step -1 Hour-	8.13	6.32	9.11	13.74	0.52	0.45	1.06	1.27
Reduced Dynamic OD 15 sec Integration Step -1 Hour-	8.14	6.28	9.08	13.72	0.52	0.45	1.07	1.27

It is easily noticed that this range of numerical integration step size change does very small effect on the reduced dynamic orbirt determination solution. The advantage of using 15 seconds of integration step size may be used in accordance with the requirements and expectations from the reduced dynamic orbit determination algorithm performed by single frequency pseudorange measurements.

3.5. ORBIT DETERMINATION SOFTWARE

3.5.1. Software Structure

Object-oriented software has been developed for the performance of the tasks accomplished within this study. The programming language has been chosen as Matlab R14 environment due to its ease of use as of being an upper level programming language and flexibility supplied for the solutions of numerical problems. On the other hand it should be noted that contrary to its ease of use as an

upper level language, Matlab has the disadvantage of being slow when compared to some lower level programming languages.

The software consists of two main routines and sub-routines. The main routines are;

reduced.m : the main routine performing reduced dynamic orbit determination
kinematic.m : the main routine performing kinematic orbit determination

and the sub-routines involve;

VW.m : computes V(nmax,nmax) and W(nmax,nmax) matrices
geoaccel.m : computes the geopotential acceleration in x,y and z directions
geocoef.m : computes the coefficient matrix (F) due to geopotential and drag acceleration
dragaccel.m : computes the acceleration caused by the drag force of the atmosphere
density.m : computes the atmospheric density by using Harris Priester density model
centrifugal.m :computes the centrifugal acceleration in x,y and z directions
coriolis.m : computes the coriolis acceleration in x,y and z directions
getephem.m : reads GPS ephemeris data
igsfile.m : returns the file name of the corresponding GPS ephemeris file
getprange.m : reads the observation data
gps2ut1.m : converts the GPS time to UT1
intlagrange.m : interpolates the GPS ephemerides to the observation epoch using Lagrangian 9 term polynomial
intSatclck.m : interpolates the coordinates of the observed GPS satellites' clock errors obtained
julian2000.m : returns the time since the epoch J2000.0
kinVel.m :calculates the current velocity of the satellite by using the estimated positions
markley.m : computes Markley's state transition matrix

CHAPTER 4

CONCLUSIONS AND RECOMMENDATIONS

4.1. CONCLUSIONS & RECOMMENDATIONS

Kinematic and reduced dynamic orbit integration methods have been implemented with the aid of software using Matlab programming language and case studies have been performed on the pseudorange code observables data simulated from the orbit solution obtained from TÜBİTAK-BİLTEN. The main objective of this study has been to apply different cases on the low earth orbiting satellite Bilsat-1 and assess the results in order to be able to achieve a reliable near real time orbit determination task within an accuracy of tens of meters by using single frequency GPS pseudorange measurements. In accordance with the objectives of the study, following results have been obtained from the tests performed on Bilsat-1 data.

With respect to the dynamical model, the tests have shown that the difference between using EGM96 geopotential model or EIGEN-CG03C model would both result in similar solutions within the expected accuracy of this study. The residuals between two solutions are within acceptable limits for the purpose of this study.

Considering the degree of the spherical harmonics to be used for orbit propagation, the coefficients up to the degree and order of 10 provided good accuracy for this study and fair computational burden when compared to the higher degree coefficients and additional accuracy that could be gained by increasing the degree and order.

In kinematic orbit determination, the tests have shown us that using rapid or final ephemerides products of IGS instead of ultra rapid ephemerides provides better

accuracy and that there is not any improvement within the scope of this study to choose between the final or rapid ephemerides.

With respect to state transition matrix of the reduced dynamic orbit determination algorithm, Markley's method of state transition provided similar results to the case where the state transition is performed by the integration of equations of motion. Implementation of Markley's method is found to be beneficial as of resulting with similar accuracy out of the Kalman filter algorithm when compared to the state transition matrix obtained from the integration of equations of motion.

The changes applied to the variables when the filter was on did not make too significant changes due to the nature of the Kalman filter. The process noise and the measurement covariance play a vital role at this step. The process noise could have been reduced in case of working with observables of more precise nature. Using single frequency pseudorange measurements for the task reduces flexibility to tune the filter for better response to the varying parameters. Keeping the system noise higher helps the system to recover the unmodelled effects in the measurement model.

It has been observed that the results from the velocity estimations have not been good enough for satellite operations. Using phase differences to overcome the effects of unmodelled forces in the measurement model would provide better results. Single phase pseudorange observables are much more dependent on the accuracy of the measurements and it may only be eliminated to some degree of accuracy by implementing Kalman filtering scheme.

Implication of an outlier detection algorithm for the kinematic orbit determination would affect the process in a positive manner as the pre-processing of the raw pseudorange data for the detection of irrelevant observations is expected to have a reflection on the estimation performance for kinematic orbit determination due to the nature of kinematic method which is so sensitive to erroneous measurements.

REFERENCES

Bisnath, S., (2004), Precise Orbit Determination of Low Earth Orbiters with a Single GPS Receiver-Based, Geometric Strategy, Ph.D. dissertation, Department of Geodesy and Geomatics Engineering Technical Report No. 220, University of New Brunswick, Fredericton, New Brunswick, Canada, 143 pp.

Chiaradia, A.P.M., Kuga, H.K.and Prado, A.F.B.A., (1999), The Use of the Single Frequence GPS Measurements to Determine in Real Time Artificial Satellite Orbits, 50th International Astronautical Congress (IAF-99-A.7.03), Amsterdam, Netherlands.

Chiaradia A.P.M., Gill E., Montenbruck O., Kuga H.K., Prado, A.F.B.A, (2000), Algorithms for On-Board Orbit Determination using GPS OBODE-GPS, DLR German Space Operations Center, Oberpfaffenhofen

Farrell J., Barth M., (1998), The Global Positioning System and Inertial Navigation, McGraw-Hill, New York, USA

Förste, C., Flechtner, F., et al. (2005), A New High Resolution Global Gravity Field Model Derived From Combination of GRACE and CHAMP Mission and Altimetry/Gravimetry Surface Gravity Data, EGU General Assembly 2005, Vienna, Austria.

Grewal M. S., Weill L. R., Andrews A. P., (2001), Global Positioning Systems, Inertial Navigation and Integration, John Wiley & Sons Inc., New York

Karslıoğlu, M.O., (2004), An Interactive Program for GPS-Based Dynamic Orbit Determination of Small Satellites, Computer & Geosciences, Vol.31, Issue 3, pp. 309-317

Kleusberg A., Teunissen P.J.G., (1996), GPS for Geodesy, Springer Verlag, Berlin, Germany

Koch K. R., (1999), Parameter Estimation and Hypothesis Testing in Linear Models, Springer Verlag, Berlin, Germany

Lemoine, F., Smith, D., et al. (1998), The Development of the Joint NASA GSFC and the National Imagery and Mapping Agency (NIMA) Geopotential Model EGM96. NASA/TP-1998-206861, Goddard Space Flight Center, Greenbelt, Maryland.

Misra, Pratap and Enge, Per, (2001), Global Positioning System, Signals, Measurements and Preformance, Ganga Jamuna Press, Massachusetts, USA, 390 pp.

Montenbruck, O. and Gill, E., (2000), Satellite Orbits, Models, Methods, Applications, Springer, Berlin, Germany, 369 pp.

Montenbruck, O., Helleputte, T., Kroes, R. and Gill, E., (2005), Reduced Dynamic Orbit Determination Using GPS Code and Carrier Measurements, Aerospace Science and Technology, Vol.9, pp.261-271.

Montenbruck, O., Helleputte, T., Kroes, R. and Gill, E., (2005), Rapid orbit determination of LEO satellites using IGS clock and ephemeris products, GPS Solut, Springer Verlag, Vol 9, pp.226-235

Orlu, U., Yüksel, G., Gomes, L., and Hall, K., (2003), Bilsat-1: Power System Sizing and Design, RAST 2003: Proceedings of the International Conference on Recent Advances in Space Technologies, İstanbul, Turkey, pp.159

Rim, J.H. and Schutz, B.H., (2002), Precision Orbit Determination, Center for Space Research, The University of Texas, Austin

Rummel, R., and Peters, T., (2001), Reference Systems in Satellite Geodesy, Institut für Astronomische und Physikalische Geodäsie, München, Germany

Seeber, G., (2003), Satellite Geodesy, Walter de Gruyter, Berlin; New York

Stenbit, J. P., Assistant Secretary of Defense for Command, Control, Communications, and Intelligence, (2001), Global Positioning System Standard Positioning Service, US Department of Defence, Washington, USA

Tapley, B. D., Schutz, B. E., and Born, G. H., (2004), Statistical Orbit Determination, Elsevier Academic Press, Burlington, USA

The International GNSS Service (IGS), (2005), IGS - International GNSS Service, formerly the International GPS Service, http://igscb.jpl.nasa.gov/index.html, 03.12.2005

Torge, W., (2001), Geodesy, de Gruyter, Berlin, Germany.

Welch G., Bishop G., (2001), An Introduction to the Kalman Filter, SIGGRAPH 2001 course 8. In Computer Graphics, Annual Conference on Computer Graphics & Interactive Techniques. ACM Press, Addison-Wesley, Los Angeles, CA, USA

Zamlutti, C. J., (1998), On the basic trends of the upper atmosphere modeling - a review, Rev. Bras. Geof., Vol.16 No.2-3

Zhou, N. and Feng, Y., (2002), Journal of Global Positioning Systems, Vol.1, No.2, pp.106-112